Atmos. Chem. Phys. Discuss., 11, 23029–23080, 2011
www.atmos-chem-phys-discuss.net/11/23029/2011/
doi:10.5194/acpd-11-23029-2011

Atmospheric Chemistry and Physics Discussions

A new multi-gas constrained model of trace gas non-homogeneous transport in firn: evaluation and behavior at eleven polar sites

E. Witrant[1], P. Martinerie[2], C. Hogan[3], J. C. Laube[3], K. Kawamura[4], E. Capron[5,6], S. A. Montzka[7], E. J. Dlugokencky[7], D. Etheridge[8], T. Blunier[9], and W. T. Sturges[3]

[1]Grenoble Image Parole Signal Automatique (GIPSA-lab), Université Joseph Fourier/CNRS, BP 46, 38 402 Saint Martin d'Hères, France
[2]Laboratoire de Glaciologie et Géophysique de l'Environnement (LGGE), CNRS/Université Joseph Fourier, BP 96, 38 402 Saint Martin d'Hères, France
[3]School of Environmental Sciences, University of East Anglia, Norwich NR4 7TJ, UK
[4]National Institute of Polar Research, 1-9-10 Kaga, Itabashi-ku, Tokyo 173-8515, Japan
[5]Laboratoire des Sciences du Climat et de L'Environnement, IPSL/CEA-CNRS-UVSQ, 91191 Gif-sur-Yvette, France
[6]British Antarctic Survey, Natural Environment Research Council, High Cross, Madingley Road, Cambridge CB3 0ET, UK

[7] NOAA Earth System Research Laboratory, Boulder, Colorado, USA
[8] Commonwealth Scientific and Industrial Research Organisation, Marine and Atmospheric Research, PMB 1, Aspendale, Vic. 3195, Australia
[9] Centre for Ice and Climate, Niels Bohr Institute, University of Copenhagen, Juliane Maries vej 30, 2100 Copenhagen Ø, Denmark

Received: 17 July 2011 – Accepted: 7 August 2011 – Published: 16 August 2011

Correspondence to: E. Witrant (emmanuel.witrant@ujf-grenoble.fr)

Published by Copernicus Publications on behalf of the European Geosciences Union.

ACPD
11, 23029–23080, 2011

Abstract

Insoluble trace gases are trapped in polar ice at the firn-ice transition, at approximately 50 to 100 m below the surface, depending primarily on the site temperature and snow accumulation. Due to the different time scales for snow accumulation versus diffusion of gases through the snowpack, age differences between gases and the ice in which they are "trapped" can be large; e.g. several thousand years in central Antarctica (a low snow accumulation area). Models of trace gas diffusion in polar firn are used to relate firn air and ice core records of trace gases to their atmospheric history. We propose a new diffusion model based on the following contributions. First, the airflow transport model is revised in a poromechanics framework with specific emphasis on the non-homogeneous properties (convective layer, depth-dependent diffusivity and lock-in zone) and an almost-stagnant behavior described by Darcy's law (gravity effect). We then derive a non-linear least square multi-gas optimization scheme to calculate the effective firn diffusivity (automatic diffusivity tuning). The improvements associated with the additional constraints gained by the multi-gas approach are investigated (up to eleven gases for a single site are included in the optimization process). The model is applied to measured data from four Arctic (Devon Island, NEEM, North GRIP, Summit) and seven Antarctic (DE08, Berkner Island, Siple Dome, Dronning Maud Land, South Pole, Dome C, Vostok) sites and the depth-dependent diffusivity profiles are calculated. Among these different sites, a relationship between an increasing thickness of the lock-in zone defined from the isotopic composition of molecular nitrogen in firn air (denoted δ^{15}N) and the snow accumulation rate is obtained, in accordance with observations. It is associated with reduced diffusivity depth-gradients in deep firn, which decreases gas density depth-gradients, at high accumulation rate sites. This has implications for the understanding of δ^{15}N of N_2 records in ice cores, in relation with past variations of the snow accumulation rate. Although the extent of layering is clearly a primary control on the thickness of the lock-in zone, our new approach that allows calculation of an estimated lock-in depth may lead to a better constraint on the age difference between the ice and entrapped gases.

ACPD

11, 23029–23080, 2011

1 Introduction

Modeling of gas transport in firns was an active field of research in the past two decades, with physical models developed and refined in parallel with measurement campaigns on ice boreholes and dedicated experimental procedures. Without pretending to be exhaustive, several key results can be mentioned here. The enclosure of air in bubbles associated with the firn sinking process was quantified by closed porosity measurements and modeled by Stauffer et al. (1985). Gas transport has first been described as a molecular diffusive process with gravitational correction by Schwander (1989). The impact of the firn sinking speed and bubble trapping was introduced simultaneously by Rommelaere et al. (1997) and Trudinger et al. (1997). The impact of thermal fractionation and turbulent transport in the convective layer (eddy flows) on the diffusion phenomenon was described by Severinghaus et al. (2001). These models were primarily focused on a diffusive process driven by a concentration gradients (Fick's law). The impact of permeability on the transport model was investigated by Schwander (1989) and Freitag et al. (2002). However, most prior work has implicitly assumed that the permeability of the firn in the region of bubble close-off was infinite, so that the air was at hydrostatic equilibrium.

Firn air transport modeling for the purpose of trace gas atmospheric history reconstructions can be decomposed into three steps. First, a physical forward model (typically referred to as the *direct model*) describes the gas transport behavior in the ice lattice, including the impact of medium heterogeneities (depth-dependent porosity, gas trapping in bubbles, localized eddy flows etc.). This results in a set of non-homogeneous partial differential equations (PDE) that has to be solved to relate the atmospheric history to the measurements at the borehole sampling date, supposing an initial gas density distribution in the firn. Six direct models of trace gas transport in firn have recently been inter-compared using a common set of input parameters (Buizert et al., 2011). The effective diffusivity appears as a key depth dependent parameter to characterize the direct model for a given firn. This parameter includes all

ACPD
11, 23029–23080, 2011

the diffusive phenomena experienced by the gas and is simply referred to as *diffusivity* in the following discussion.

Fabre et al. (2000) compared experimental and inverse model based diffusivity profiles and concluded that firn diffusivity is more influenced by macro-structure scale than micro-structure scale features measured on small samples (i.e. 4 cm). The second step is thus to identify the diffusivity depth profile using measured gases for which the atmospheric history is known (measured or obtained from atmospheric models). The associated model is defined by the combination of the direct model, gas history, borehole measurements and identification method, and is typically termed as the *inverse diffusivity model*, as it is the solution of an inverse problem from a mathematical point of view (see e.g. Rommelaere et al., 1997; Trudinger et al., 2002; Buizert et al., 2011).

The third and last step is to make use of the previous model to reconstruct the atmospheric history of gases for which only firn air measurements are available, possibly correlating the results obtained at different polar sites. Indeed, reconstructing trace gas concentration trends prior to their atmospheric measurement period is a major motivation for firn air analysis (see e.g. Montzka et al., 2011, and references therein). We may refer to such models as inverse atmospheric history models, as an underlying automatic method is used to reconstruct gases history (in comparison with the alternative method of just comparing direct firn model results with data). Several methods were developed for that purpose: Green function based (Rommelaere et al., 1997), Monte-Carlo based (Bräunlich et al., 2001), or effective age based (Trudinger et al., 2002). These methods were recently applied, for example, to HFC-227ea (1,1,1,2,3,3,3-Heptafluoropropane, Laube et al., 2010), mercury (Faïn et al., 2009) and HFC-23 (Trifluoromethane, Montzka et al., 2010) respectively. Alternatively, trace gas concentration trends can be assessed from their atmospheric budgets and compared to firn data by using a direct firn model (e.g. Butler et al., 1999; Martinerie et al., 2009; Montzka et al., 2010).

Our goals in this paper are to analyze the transport phenomena associated with the direct model, in order to build a more physically realistic inverse diffusivity model based

ACPD
11, 23029–23080, 2011

on multiple gases, which is evaluated at eleven polar sites. The modeling constraints and assumptions are motivated by the multi-sites inverse scenario model perspective.

The physical transport model adds Darcy's Law to the treatment of firn gas transport in a poromechanics framework, starting from mass conservation in an interconnected network (ice lattice, gas connected to the surface and gas trapped in bubbles) and is described in Sect. 2. The problem formulation and optimization aspects associated with the inverse diffusivity model are then considered in Sect. 3, along with evaluation of the efficiency of the method and the impact of key parameters. Eleven modeled polar sites are finally compared in Sect. 4, showing a snow accumulation rate dependent behavior.

2 Physical model and hypotheses

The aim of this section is to describe a new model of trace gas non-homogeneous transport in firns columns from mass conservation and fundamental physical laws. This is achieved by considering the firn as an interconnected network of ice, free air and air trapped in bubbles. The interconnections are constrained by conservation laws in porous media. Several issues associated with the transport characterization are detailed, as well as simplifying hypotheses that allow the use of this model for multi-gas diffusivity optimization.

2.1 Mass conservation and interconnected network

The conservation of mass, both for ice and gases, can be described by considering the firn as composed of a sinking solid structure (ice) and of a transported fluid (air and trace gases). The fixed reference frame is considered to be the snow surface. The space available for the fluid is composed of the open pores (having a free path to the surface) and the closed pores (sinking with the firn), which constitute a network of two spaces interconnected through the rate of fluid mass transferred from one space to

ACPD
11, 23029–23080, 2011

the other. The dynamics of such a system is inferred from the mass conservation law combined with poromechanics (Coussy, 2003) as (Eulerian continuity):

$$\begin{cases} \dfrac{\partial[\rho_{\text{ice}}(1-\epsilon)]}{\partial t} + \nabla[\rho_{\text{ice}}(1-\epsilon)\boldsymbol{v}] = 0 \\ \dfrac{\partial[\rho_{\text{f}}^{\text{o}} f]}{\partial t} + \nabla[\rho_{\text{f}}^{\text{o}} f(\boldsymbol{v}+\boldsymbol{w}_{\text{f}})] = -\boldsymbol{r}^{\text{o}\to\text{c}} - \lambda\rho_{\text{f}}^{\text{o}} \\ \dfrac{\partial[\rho_{\text{f}}^{\text{c}}(\epsilon-f)]}{\partial t} + \nabla[\rho_{\text{f}}^{\text{c}}(\epsilon-f)\boldsymbol{v}] = \boldsymbol{r}^{\text{o}\to\text{c}} - \lambda\rho_{\text{f}}^{\text{c}} \end{cases}$$

where ρ_{ice} is the ice density, $\rho_{\text{f}}^{\text{o}}$ the fluid density in open pores, $\rho_{\text{f}}^{\text{c}}$ the fluid density in closed pores, ϵ the total porosity (pores volume/firn layer volume), f the open porosity (open pores volume/firn layer volume), $\boldsymbol{v}$ the firn sinking speed, $\boldsymbol{w}_{\text{f}}$ the relative fluid speed with respect to the firn and $\boldsymbol{r}^{\text{o}\to\text{c}}$ the rate of fluid mass going from the opened to the closed pores. The "f"subscript generically denotes the fluid considered (air or trace gas in our case). $\partial/\partial t$ denotes the partial derivative with respect to time and ∇ is the gradient operator in 3-D space. The main notations are summarized in Table 1 of the Supplement. A radioactive decay with rate λ can possibly be considered, if such mass loss occurs for a specific gas (for unstable species, e.g. $^{14}CO_2$).

Supposing that the main transport phenomena occur in the vertical direction, denoted as z, the previous model may be written in the 1-D form:

$$[\rho_{\text{ice}}(1-\epsilon)]_t + [\rho_{\text{ice}}(1-\epsilon)v]_z = 0 \tag{1a}$$

$$[\rho_{\text{f}}^{\text{o}} f]_t + [\rho_{\text{f}}^{\text{o}} f v]_z + [\rho_{\text{f}}^{\text{o}} f w_{\text{f}}]_z = -r_{\text{f}}^{\text{o}\to\text{c}} - \lambda\rho_{\text{f}}^{\text{o}} \tag{1b}$$

$$[\rho_{\text{f}}^{\text{c}}(\epsilon-f)]_t + [\rho_{\text{f}}^{\text{c}}(\epsilon-f)v]_z = r_{\text{f}}^{\text{o}\to\text{c}} - \lambda\rho_{\text{f}}^{\text{c}} \tag{1c}$$

ACPD
11, 23029–23080, 2011

where the subscripts t and z denote the time and space partial derivatives, respectively, and v, w_f and $r_f^{o\to c}$ (positive downward) are the z-components of $\boldsymbol{v}$, $\boldsymbol{w}_f$ and $\boldsymbol{r}^{o\to c}$, respectively.

The 1-D representation implies a layer-averaged description of the transport phenomena (horizontal firn isotropy hypothesis). The major depth-variation of the transport parameters (vertical variation due to e.g. firn densification process, seasonality or melt layers) can be represented. This vertical anisotropy was observed to be a major 3-D property of polar firn by e.g. Hörhold et al. (2009) using X-ray microtomography. The main limitation of the 1-D assumption is the lack of representation of the effect of cracks or size limits of horizontal impermeable layers.

2.2 Firn sinking speed and porosities

In order to calculate the firn sinking speed and porosities from the available data, the following assumptions are necessary: (1) the temperature and pressure variations have a negligible effect on the density of pure ice (ρ_{ice} is constant), (2) the variations of the snow accumulation rate have a negligible impact on the firn dynamics (Eq. (1aa) is considered at steady-state), (3) the firn bulk density profile $\rho_{firn}(z)$ is smooth and monotically increasing with depth (the layering is neglected). These assumptions are particularly important for the deep firn modeling. A direct consequence is that the open and closed porosities are constant over time (space-dependency only) and the firn sinking speed is obtained by solving the boundary-value problem (BVP):

$$[\rho_{ice}(1-\epsilon(z))v(z)]_z = 0, \quad \rho_{ice}(1-\epsilon(0))v(0) = a_{accu}$$

where a_{accu} is the surface accumulation rate of snow (mass flow rate per unit area). The firn sinking speed is then $v(z) = a_{accu}/[\rho_{ice}(1-\epsilon(z))]$.

The total porosity is calculated from $\rho_{firn}(z)$ and ρ_{ice}, with the temperature-dependent ice density proposed by Schwander et al. (1997), as:

ACPD
11, 23029–23080, 2011

$$\rho_{ice} = 916.5 - 0.014438(T - 273) - 0.00015175(T - 273)^2$$
$$\epsilon(z) = 1 - \rho_{firn}(z)/\rho_{ice}$$

where T is the site temperature.

The open porosity f is set by the close-off density ρ_{co} (density at which $f/\epsilon = 0.37$). The computation proposed by Goujon et al. (2003) is slightly modified as ρ_{co} is obtained by specifying the full close-off depth independently for each site and solving:

$$\epsilon_{co} = 1 - \rho_{co}/\rho_{ice}$$
$$f(z) = \epsilon(z)(1 - 0.37\,(\epsilon(z)/\epsilon_{co})^{-7.6})$$

2.3 Trace gases and the advective-diffusive model

The individual mass fluxes of a gas mixture "gm" or the correction factors proposedcan be evaluated with the filtration vector $\phi_x = f w_x$ (where x denotes the gas mixture, air or a trace gas, and w is the flow speed relative to the firn lattice) as:

$$\phi_{gm} = \chi_{air}\phi_{air} + \sum_{i=1}^{N_g} \chi_{\alpha_i}\phi_{\alpha_i}$$

where N_g is the number of trace gases, χ_x is the mole fraction of gas x in the gas mixture and α_i denotes the specific gas i. The specific filtration vector is then:

$$\phi_{\alpha_i} = \phi_{gm} + \left(\chi_{air} + \sum_{j\neq i} \chi_{\alpha_j}\right)\phi_{\alpha_i} - \chi_{air}\phi_{air} + \sum_{j\neq i} \chi_{\alpha_j}\phi_{\alpha_i} \approx \phi_{air} + \chi_{air}(\phi_{\alpha_i} - \phi_{air}) \quad (2)$$

where the last approximation is obtained from the hypotheses that the gas is mainly air (trace gas hypothesis) and that the gases do not affect each others (no chemical reaction).

ACPD
11, 23029–23080, 2011

In the classical advective-diffusive model (ADM) ϕ_{air} is the advection with air (Darcy's law) and $\chi_{\text{air}}(\phi_{\alpha_i} - \phi_{\text{air}})$ is the molecular diffusion described by Fick's law. While the ADM is particularly easy to use, its accuracy was discussed and finer results may be obtained with the dusty gas model (DGM, thoroughly described by Mason and Malinauskas, 1983 or Cunningham and Williams, 1980) or the correction factors proposed by Webb and Pruess (2003). The improvement brought by the DGM is due to the fact that it takes into account the couplings between ordinary diffusion, Knudsen diffusion and advection. As the aim of this paper is to identify the firn diffusivity profile in a multi-gas model, the general structure of the ADM model is kept for its simplicity (linearity in the diffusivity coefficient) and modified to take into account the stagnant/nonstagnant distinction discussed in Sect. 2.5. Note that the gas is considered as stagnant with respect to its environment when it does not move with respect to the reference frame (stratified state at equilibrium).

2.4 Advection-driven diffusion: Darcy's law

The gas motion induced by external or internal forces (momentum conservation) can be introduced in the mass conservation equation according to Darcy's law (the flux is linearly related to the applied forces):

$$f w_{\text{f}} = \frac{\kappa_{\text{f}}}{\mu_{\text{f}}}(-[P_{\text{f}}]_z + \rho_{\text{f}} g) = \frac{\kappa_{\text{f}}}{\mu_{\text{f}}}\left(-\frac{RT}{M_{\text{f}}}[\rho_{\text{f}}]_z + \rho_{\text{f}} g\right) \quad (3)$$

where $\kappa_{\text{f}}(z)$ is the firn permeability, μ_{f} the dynamic viscosity, P_{f} the fluid pressure, R the ideal gas constant, g the acceleration due to gravity and M_{f} the molar mass. The right-hand equality is obtained by supposing that each trace gas behaves as an ideal gas and that the effect of thermal flows can be neglected (the inclusion of a temperature gradient is mentionned in the Supplement).

Without the phenomena of firn sinking and gas trapping in bubbles phenomena, Eq. (1ab) combined with Eq. (3) at steady-state provide the fluid hydrostatic equilibrium density $\bar{\rho}_{\text{f}}$ as:

ACPD
11, 23029–23080, 2011

$$-\frac{RT}{M_f}[\bar{\rho}_f]_z + \bar{\rho}_f g = 0 \quad \Leftrightarrow \quad \bar{\rho}_f(z) = \rho_f(0) e^{\frac{M_f g}{RT} z}$$

where $\rho_f(0)$ is the atmospheric density at the surface.

In fact, taking into account firn sinking and gas trapping, the hydrostatic equilibrium is not achieved. Darcy's law then describes the flux induced by a deviation $\tilde{\rho}_f$ from hydrostatic equilibrium as:

$$f w_f = \frac{\kappa_f}{\mu_f}\left(-\frac{RT}{M_f}[\tilde{\rho}_f]_z + \tilde{\rho}_f g\right) \tag{4}$$

with $\tilde{\rho}_f = \rho_f - \bar{\rho}_f$. This transport phenomenon describes the behavior of air at steady-state and trace gases at quasi steady-state.

2.5 Molecular diffusion: Fick's law

The relative motion of a trace gas α with respect to air is affected by molecular diffusion according to Fick's law:

$$f \chi_{air} \chi_\alpha (w_\alpha - w_{air}) = -D_\alpha [\chi_\alpha]_z$$

where χ_{air} and χ_α are the mole fractions of air and gas α, respectively. $D_\alpha(z)$ is the effective molecular diffusivity of gas α. For a stagnant gas this diffusivity is related to the inverse of the tortuosity $v(z)$ and the gas diffusion coefficient in free air $D_{\alpha,g}$ with $D_\alpha = f v D_{\alpha,g}$ according to van Deemter et al. (1956). Nevertheless, the specific analysis carried by Fabre et al. (2000) concluded that the tortuosity profiles measured on small firn samples cannot be used directly to determine the diffusivities inferred from inverse diffusivity models. The effective diffusivity, instead of tortuosity, is thus kept as the free parameter of interest in our analysis.

ACPD
11, 23029–23080, 2011

Supposing that the ambient gas is mainly composed of air ($\chi_{air} \approx 1$ and $\chi_\alpha \approx M_{air}\rho_\alpha / M_\alpha \rho_{air}$), Fick's law writes in terms of densities (in terms of mass per unit volume) as:

$$f\rho_\alpha(w_\alpha - w_{air}) = -D_\alpha \left([\rho_\alpha]_z - \rho_\alpha \frac{[\rho_{air}]_z}{\rho_{air}} \right) \quad (5)$$

Note that, while Fick's law is reasonably accurate to describe the molecular diffusive flux for a nonstagnant gas, it was found to be totally inadequate for a stagnant gas (considered as a gas without source or sink, thus at steady state), as discussed by Thorstenson and Pollock (1989). Note also that Fick's Law is adequate for a trace gas, but for a major gas the Stefan-Maxwell equations (diffusion in a multi-component system) must be used. This implies, in the framework of trace gas transport in firns, that Fick's law is suitable to describe the dynamics of gases with large atmospheric variations in nonstagnant firn regions but should be used with care otherwise (small concentration gradients or limited airflow in deep firn). Transport in the "almost stagnant" case (where the hydrostatic equilibrium is not fully reached) is then considered as being driven by external forces in combination with the classical Fick behavior, using Darcy's law to describe the fluid (air and trace gases) behavior at steady-state.

2.6 Air transport and bubble trapping

As discussed previously the transport of gases with constant atmospheric concentration (the dynamics (1ab–1ac) are at steady-state) is mainly driven by a Darcian flux. Considering air transport (no diffusion) and supposing a constant atmospheric pressure (or at least a constant mean pressure), the air density is set according to Eqs. (1ab) and (4) as:

$$[\rho^o_{air} f v]_z + \left[\rho^o_{air} \frac{\kappa_{air}}{\mu_{air}} \left(-\frac{RT}{M_f} [\tilde{\rho}^o_{air}]_z + \tilde{\rho}^o_{air} g \right) \right]_z = -\rho^o_{air} \tau$$

ACPD
11, 23029–23080, 2011

where $\tau(z) = -v\epsilon[f/\epsilon]_z$ is the rate of gas volume exchange between the open and closed networks, according to the air trapping model proposed by Rommelaere et al. (1997). The trapping phenomenon could be completed with the selective permeation of gases depending on the effective molecular diameters proposed by Severinghaus and Battle (2006). This process applies to atoms and molecules of small diameter, which is not the case for the gases considered in our study.

A direct approach to this problem would require a knowledge of the firn permeability (scaling laws such as those proposed by Schwander (1989) or Freitag et al. (2002) could be used for this purpose) and would require solution of a nonlinear BVP, which would necessitate a dedicated mathematical analysis (our tests using classical commercial solvers failed to provide satisfactory results). An alternative is to suppose a small deviation of the air density with respect to the hydrostatic profile ($\rho^{o}_{air} \approx \bar{\rho}^{o}_{air}$) and to choose $w_{air}(z)$ as the independent variable, obtained by solving the linearized BVP:

$$[\bar{\rho}^{o}_{air} f v]_z + \left[\bar{\rho}^{o}_{air} f w_{air}\right]_z = -\bar{\rho}^{o}_{air}\tau, \quad w_{air}(z_f) = 0$$

where z_f denotes the bottom of the firn and w_{air} is the relative air flow speed induced by the variation $\tilde{\rho}^{o}_{air}$. The advantage of this approach (previously used by Rommelaere et al., 1997) is to provide $w_{air}(z)$ without the momentum conservation equation but the drawback is to necessitate a hydrostatic profile for the air density. This may be a strong hypothesis in the gas trapping region, where neglected local pressure gradients (e.g. induced by surface stress and capillary pressure, see Coussy, 2003) may alter the natural hydrostatic pressure distribution. Nevertheless, we consider the hydrostatic air distribution as a necessary condition for the direct model, and the solution of the BVP is:

$$w_{air}(z) = \frac{1}{\bar{\rho}^{o}_{air}(z) f(z)} \int_z^{z_f} \left(\bar{\rho}^{o}_{air}\tau + [\bar{\rho}^{o} f v]_z\right) dz$$

ACPD
11, 23029–23080, 2011

The air trapped in closed pores ρ^{c}_{air} is directly obtained from Eq. (1ac) at steady-state as:

$$[\rho^{c}_{air}(\epsilon - f)v]_z = \rho^{o}_{air}\tau, \quad \rho^{c}_{air}(0) = \rho^{atm}_{air}$$

with $\rho^{o}_{air} \approx \bar{\rho}^{o}_{air}$ and can be evaluated by the air content computation:

$$\text{Air Content} = \frac{n^{c}_{air}}{n^{atm}_{air}} \frac{1}{\rho_{firn}} = \frac{\epsilon - f}{1 - \epsilon} \frac{\rho^{c}_{air}}{\rho^{atm}_{air}} \frac{1}{\rho_{ice}}$$

where n denotes the molar density. The air content may be compared to experimental data (e.g. in Martinerie et al., 1994).

2.7 Turbulent flows and eddy diffusivity

The flow in the upper layer of the firn experiences faster transients due to the suction effect of the wind, the seasonal temperature gradients and the higher porosity. Its behavior is thus mainly turbulent and the gas dynamics in the upper region can be modeled by introducing an eddy component (random motion of volumes of fluid) in the diffusivity description D_{eddy}, as proposed by van Deemter et al. (1956) for the theoretical analysis of turbulent diffusion in a chromatography column and considered in the firn framework by Arnaud (1997). Supposing constant (space-independent) permeability and porosity and considering a Darcian motion of the airflow, Colbeck (1989) described wind pumping as a purely diffusive pressure perturbation where the diffusion term is proportional to the air pressure. Colbeck solved a simplified analytical 2-D model for air velocity, which declined exponentially with depth. This motivated the use of a D_{eddy} term that is characterized by an exponential decay with depth by Severinghaus et al. (2001) (see Severinghaus et al., 2010, for more details on the analysis of this phenomenon).

An alternative is to set an upper bound on the maximum admissible molecular CO_2 diffusivity D_{air} (in free air) and define the effective eddy flow depth z_{eddy} as the depth

ACPD
11, 23029–23080, 2011

above which $D_\alpha \geq \varrho_\alpha \alpha_c D_{air}$ (where ϱ_α denotes the relative diffusivity of gas α with respect to the one of CO_2 and α_c is a correction factor that takes into account the upper firn porosity). For the purpose of our model, the important issue is that D_{eddy} does not depend on the gas considered and is typically much larger than the molecular diffusivity. This phenomenon can be modeled by introducing an extra term in the diffusivity that does not depend on the specific gas considered and the overall diffusivity is defined as:

$$D_\alpha = \begin{cases} D_{eddy} + \varrho_\alpha \alpha_c D_{air} & \text{if } z \leq z_{eddy} \\ \varrho_\alpha D_{CO_2} & \text{if } z > z_{eddy} \end{cases} \quad (6)$$

where $D_{CO_2}(z)$ is the CO_2 diffusivity profile in the firn. The transition between molecular and eddy diffusivity is obviously progressive and would need an extra, space-dependent, ratio term (such as a sigmoid curve instead of an abrupt transition).

Considering the inverse diffusivity model framework (where an optimization algorithm iterates on D_α to minimize some criteria, thus providing D_{eddy} and D_{CO_2} as outputs), z_{eddy} can be automatically determined as the depth at which $D_\alpha(z_{eddy}) = \varrho_\alpha D_{air}$.

2.8 Trace gas transport

The trace gas dynamics is set according to the mass conservation (1ab), trace gas flux (2), molecular diffusion (5) and advection with air as (setting $\chi_{air} = 1$):

$$\begin{cases} [\rho^o_\alpha f]_t + [\rho^o_\alpha f(v + w_{air})]_z + \rho^o_\alpha(\tau + \lambda) - \left[D_\alpha \left([\rho^o_\alpha]_z - \rho^o_\alpha \dfrac{[\rho_{air}]_z}{\rho_{air}} + \mathcal{A}_{ss} \right) \right]_z = 0 \\ \rho^o_\alpha(0,t) = \rho^{atm}_\alpha(t) \\ \dfrac{RT}{M_f}[\rho^o_\alpha(z_f,t)]_z - \rho^o_\alpha(z_f,t) = 0 \end{cases} \quad (7)$$

where $\mathcal{A}_{ss}(z)$ is included to take into account the limitations of Fick's law and sets the steady-state behavior. $\mathcal{A}_{ss}$ has implicitly been used in previous works to include the

ACPD
11, 23029–23080, 2011

gravity effect (following the gravitational correction of the diffusion flux proposed by Schwander, 1989). We use this term here in two different ways: (1) to include the local effect of internal or external forces on the trace gas (with Darcy's law), denoted with $A_{ss}(z)$, and (2) to describe the global distribution $\mathcal{A}_{ss}$ (which extends over the whole depth) that can contain alternatively some regions where the forces compensate each other (such as the convective region and possibly the lock-in zone (LIZ), in this case $\mathcal{A}_{ss} = 0$ for the corresponding depths) and some regions where Darcy's law apply ($\mathcal{A}_{ss} = A_{ss}$). This distinction is made to compare different approximations of Darcy's law and the choices that can be made on a specific region behavior, as discussed in the next section based on experimental data.

A direct approach to include the local effect of internal or external forces in the model would necessitate the permeability depth-distribution, as discussed for air in Sect. 2.6. An alternative is to consider that the fluxes induced by molecular and advection-driven diffusion are balanced at equilibrium, and that the impact of forces on the trace gas is reflected by its advection speed. Supposing that the viscous effects described by Darcy's law dominate in almost-stagnant regions ($[\rho^o_\alpha f]_t \approx 0$) and denoting as $A_{ss,D}(z)$ the value of $\mathcal{A}_{ss}$ in these regions, $A_{ss,D}$ has to ensure that the flux term converges towards the stagnant equilibrium:

$$-D_\alpha \left([\rho^o_{\alpha,ss}]_z - \rho^o_{\alpha,ss} \frac{[\rho_{air}]_z}{\rho_{air}} + A_{ss,D} \right) = \rho^o_{\alpha,ss} f (w_\alpha - w_{air})$$

$$\Leftrightarrow A_{ss,D} = -\frac{\rho^o_{\alpha,ss} f}{D_\alpha}(w_\alpha - w_{air}) - \left([\rho^o_{\alpha,ss}]_z - \rho^o_{\alpha,ss} \frac{[\rho_{air}]_z}{\rho_{air}} \right)$$

where $\rho^o_{\alpha,ss}(z)$ is the stagnant trace gas density. The steady-state expression of Darcy's law provides $\rho^o_{\alpha,ss}$ by linearizing the associated BVP around the hydrostatic density distribution, as detailed for air in Sect. 2.6. However, the definition of a steady-state profile for trace gases with a time-varying atmospheric concentration introduces important errors and a quasi-steady state (QSS) approach should be preferred. In that case $\rho^o_{\alpha,ss}$ is replaced by ρ^o_α (the steady-state value of the density is updated with the actual value)

ACPD
11, 23029–23080, 2011

and w_α is calculated with the hydrostatic pressure distribution of the trace gas combined with gas trapping and firn sinking. This hypothesis is verified as time-variations of the density induce a relatively important concentration gradient $[\rho^{\circ}_{\alpha}]_z$, which renders $\mathcal{A}_{ss}$ negligible in the transport Eq. (7). The QSS approach implies:

$$A_{ss,D} \approx \rho^{\circ}_{\alpha} \left[\left(\frac{[\rho_{air}]_z}{\rho_{air}} - \frac{[\rho^{\circ}_{\alpha,ss}]_z}{\rho^{\circ}_{\alpha,ss}} \right) - \frac{f}{D_\alpha} (w_\alpha - w_{air}) \right]$$

Neglecting the flow speed difference $w_\alpha - w_{air}$ (supposing that the trace gas advection is fully determined by air and the trapping phenomenon τ does not depend on the gas) and approximating $[\rho^{\circ}_{\alpha,ss}]_z$ as $M_\alpha g/RT \times \rho_{\alpha,ss}$ provide the simplified expression:

$$A_{ss,sim} = \rho^{\circ}_{\alpha} \left(\frac{[\rho_{air}]_z}{\rho_{air}} - \frac{M_\alpha g}{RT} \right)$$

where ρ_{air} is approximated by the hydrostatic air distribution. This approximation is consistent with previous models (Rommelaere et al., 1997; Trudinger et al., 1997; Severinghaus et al., 2010), as discussed in the Supplement. Our detailed analysis clearly identifies the necessary physical hypotheses, to test their respective importance in comparison with the experimental results (next section) and to analyze the macroscopic behavior of trace gases in the LIZ (Sect. 4.1). It also appears as an important issue to define the convective layer (which differs from the other models) and possibly the LIZ, introduced as follows.

The final distribution of $\mathcal{A}_{ss}$ reflects the non-homogeneous quality of transport in the different firn regions as:

- a diffusive behavior in the convective layer dominated by turbulent exchanges with overlying atmosphere (which prevents gravitational and thermal fractionation from occurring);
- combined molecular diffusion and Darcy's equilibrium in the middle part of the firn, where gravitational fractionation has a significant impact;

ACPD
11, 23029–23080, 2011

– possibly a simplified transport in the LIZ where the advection is only determined by firn sinking and bubble trapping (limited gravity impact through the advection-driven diffusion term, $\mathcal{A}_{ss} \approx 0$).

According to these observations, the trace gas dynamics is set with the diffusivity defined in Sect. 2.7 (with or without D_{eddy}), the variation law (7) and

$$\mathcal{A}_{ss,1} = \begin{cases} 0 & \text{if } z \le z_{conv} \\ A_{ss,D} & \text{if } z_{conv} < z \le z_{lid} \\ 0 & \text{if } z_{lid} < z \end{cases} \quad (8)$$

where z_{lid} denotes the lock-in depth. The choice of $\mathcal{A}_{ss} = 0$ below z_{lid} implies that the internal and external forces have a negligible impact on trace gases in the vertical direction, which is the case if the surface stress tensor or non-vertical pressure gradients dominate the gravitational force in the LIZ. The stress tensor is induced by the firn deformation gradient (Coussy, 2003) and local pressure gradients that may appear if thin walls enclosing a pressurized bubble break, two phenomena associated with the bubble closure process. Alternatively, supposing that the transport in the LIZ can be represented by the QSS approach, the following model may be used:

$$\mathcal{A}_{ss,2} = \begin{cases} 0 & \text{if } z \le z_{conv} \\ A_{ss,sim} & \text{if } z_{conv} < z \end{cases} \quad (9)$$

and the convective layer depth can be automatically computed according to Eq. (6). The next section discusses the representation of experimental data obtained with the above transport descriptions.

2.9 Multi-gas transport at NEEM and Vostok

The different choices for the transport specification described in Sect. 2.8 are evaluated at two sites: NEEM, which is the best constrained in terms of number of available trace gases for diffusivity calculation (Buizert et al., 2011), and Vostok, at which a deep convective zone is observed (Bender et al., 1994). The datasets associated with both sites

ACPD
11, 23029–23080, 2011

are described in the Supplement. The specific choice of these two sites is motivated by the very different surface conditions, in terms of temperature and accumulation rate, thus providing a large spectrum for the model behavior. This evaluation involves the calculation of an optimal diffusivity profile (described in Sect. 3) for each transport case. Two types of quality indications are used here: (1) the root mean square deviation (RMSD, defined as in Eq. 10) between model results and firn data for the species used in diffusivity calculation (reference gases), which have varying atmospheric trends (as discussed in Sect. 3.4), and (2) the comparison of model results with isotopic indicators of firn transport (δ^{15}N: ^{15}N^{14}N vs. ^{14}N^{14}N, δ^{40}Ar: ^{40}Ar vs. ^{36}Ar, δ^{86}Kr: ^{86}Kr vs. ^{82}Kr). The second indicators are constant gases (with constant atmospheric concentrations), which fractionate in firn due to the mass difference between the major and minor isotope (see e.g. Landais et al., 2006; Severinghaus et al., 2010). The different transport configurations, illustrated in Fig. 1 and Table 1, are denoted with the index ζ.

The first three cases ($\zeta = \{0, 1, 2\}$) use the same transport formulation over the whole firn, without specific representations for the convective and lock-in zones. Choosing only Fick's law ($\zeta = 0$, $A_{ss} = 0$) does not allow us to represent the gravitational fractionation of inert gases (Fig. 1) and leads to a poor fit of reference gases in terms of RMSD at NEEM (Table 1). Choosing only Darcy's law ($\zeta = 1$, quasi-steady state expression: $A_{ss,D}$) provides the best RMSD at NEEM but does not allow the absence of isotopic fractionation in the convective zone and the LIZ for inert gases to be represented. Gravitational fractionation occurs throughout the firn as the treatment of Darcy's law includes gravity as an external force exerted on the gases. Nevertheless, inert gas data indicate that such fractionation does not occur in the convective and lock-in zones. The approximation $A_{ss,sim}$ ($\zeta = 2$) leads to a similar RMSD and correctly represents the behavior of inert gases in the LIZ. The "flattening effect" of the LIZ naturally appears with the hypothesis that the trace gas advection is fully driven at steady state by the one of air ($w_\alpha = w_{air}$). It means that the speed of trace gases (which would require introducing the momentum conservation for a rigorous analysis) can be satisfactorily approximated by the air flow speed. The incomplete flatness of the LIZ results

ACPD
11, 23029–23080, 2011

from the specific equilibrium between gravity and molecular diffusion occurring in this region. Forcing the flattening by setting $\mathcal{A}_{ss,1}$ (zero in the LIZ, $\zeta = 3$) provides also a valid solution but necessitates the lock-in depth to be specified. Overall, excluding the pure Fickian formulation, the choice of transport formulation ($\zeta = \{1, 2, 3\}$) has an insignificant impact on the quality of the results for references gases (equivalent RMSDs) but mostly affects the representation of inert gas isotopes. The simplified formulation $\mathcal{A}_{ss,sim}$ ($\zeta = 2$) predicts the lock-in depth while providing a simpler (less computationally intensive) model. It is thus used in the reference simulation ($\zeta = 7$).

Other transport tests ($\zeta = \{4, 5, 6, 7\}$) focus on the convective zone formulation. The first test ($\zeta = 4$, $\mathcal{A}_{ss,2}$) introduces the absence of gravitational fractionation in the convective zone. The underlying assumption is that, as in the atmosphere, turbulent transport is fast enough to prevent the occurrence of gravitational fractionation. As turbulent transport (related to e.g. surface wind and pressure variations) is not explicitly represented in firn models, z_{conv} is imposed in order to fit the behavior of inert gases (4 m (Buizert et al., 2011) at NEEM and 13 m (Bender et al., 1994) at Vostok). This allows us to simulate the (isothermal) behavior of δ^{15}N, δ^{86}Kr and δ^{40}Ar in firn (see Fig. 1; δ^{15}N at Vostok is illustrated in Sect. 4). It has a limited impact on reference gases at NEEM whereas it strongly affects RMSD at Vostok, where the convective zone is much deeper. The last step is to introduce the fact that the molecular diffusion can not exceed the one in free air ($\zeta = 5$), possibly corrected ($\zeta = 7$, α_c factor) to take into account the upper firn porosity effect, as suggested by Severinghaus and Battle (2006). When the diffusivity exceeds this threshold (above z_{eddy}), the diffusive phenomenon is considered similar to the one of an eddy flow (same diffusion coefficient for all gases). The correction factor that takes into account the porosity effect on the diffusivity threshold (α_c) reduces the offsets observed on isotopes in the LIZ. When the threshold depth for gravitational fractionation (z_{conv}) is not modified ($\zeta = \{5, 7\}$), inert gases are not affected and the impact on reference gases (RMSD) is small. By contrast, modifying z_{conv} to make it consistent with the diffusivity threshold depth calculated by the model z_{eddy} (where the identified diffusivity becomes larger than the one in free air corrected by ϱ_α,

ACPD
11, 23029–23080, 2011

10.6 m at NEEM) more significantly increase the RMSD and reduces the fit of CH_3CCl_3 and HFC-134a data in the upper firn with respect to the reference simulation (Fig. 1). The eddy flow theory predicts that the diffusivity should be much larger (more than 3 or 4 times Anderson, 1991) than the molecular one in the eddy region, which is not observed here. Transient phenomena (such as the variations of the atmospheric pressure and accumulation rates, temperature gradients or the surface winds) may also explain the increased diffusivity in the upper region. A more detailed surface analysis, such as the one proposed by Hörhold et al. (2009) and references therein, would probably be required to define an appropriate physical model for this region.

Comparing the diffusivity profiles for the different test cases (top-left subplot in Fig. 1), most of the differences occur in the upper firn (up to 20 m from the surface), except for the Fick-only transport. These variations have a limited impact on the final concentration distribution of reference gases. The diffusivities in the lower firn (which have a larger impact on the inverse scenario model) are very close and thus probably more affected by the mass conservation property and gas trapping description of our model than by the quasi-stagnant description (which mostly affects inert gases).

2.10 Impact of the numerical integration scheme

Several issues associated with the transport model discretization are detailed in the Supplement. The main conclusions of this analysis are that Lax-Wendroff and first-order upwind methods can safely be used for the discretization of first order space-derivatives, and successive approximations of the solution with $\Delta z = \{0.8, 0.4, 0.2\}$ m do not induce major numerical discrepancies, the scheme stabilizing between $\Delta z = 0.4$ and 0.2 m. The second order space-derivatives are discretized with a central difference scheme. Implicit time discretization with a sampling time of $t_s = 1$ week provides a good trade-off between numerical accuracy and simulation time (similar results as for $t_s = 1$ day while $t_s = 1$ month significantly differs). An explicit scheme with $\Delta z = 0.2$ m requires a computation time almost 500 times larger than the implicit model and is thus not suited for optimization procedures involving multiple calls of the direct model. A

ACPD
11, 23029–23080, 2011

mixed implicit-explicit scheme (Crank-Nicholson) provides similar results as the implicit scheme, but induced numerical instabilities in specific tests with the inverse scenario model.

2.11 Conclusions and perspectives

The proposed mass conservation relationships have the advantage of clearly identifying the different subsystems involved in firn mass transport modeling and their interactions. The focus on advection-driven diffusion allowed for introducing the external forces, such as gravity, in the classical molecular diffusion framework. We could introduce this phenomenon despite the lack of information on permeability with the quasi-steady state hypothesis and the fact that the associated term in the transport equation plays a significant role only when the trace gas density profile becomes constant. The limitations of Fick's law to represent almost-stagnant behavior could thus be compensated and the peculiar transport of gases with constant atmospheric behavior is well represented by the model without setting a specific LIZ depth (the flattening effect seen in isotopes of inert gases in the lock-in region is captured by the almost-stagnant description).

As the D_{eddy} concept does not improve our representation of the convective zone, an alternative could be to evaluate the effect of introducing a variable surface pressure (statistically representative of atmospheric variations). The pressure variations due to wind stress on a non-flat surface are more difficult to represent, but may affect strongly only sites undergoing a high surface rugosity such as Megadunes (Severinghaus et al., 2010).

Our specific QSS approach to describe the almost stagnant firn regions can be more generally considered in the framework of trace gas transport in porous media (applications in contaminant migration and removal, evaporation and drying, porous catalysts or gas nuclear reactors, as mentioned by Webb and Pruess, 2003). It has the advantage to improve the ADM behavior without information on permeability and to involve simple expressions for the diffusivity term (contrarily to the DGM), which allows for

ACPD
11, 23029–23080, 2011

inverse modeling objectives. Future research would be needed to compare the relative performance and limitations of the proposed approach.

3 Inverse diffusivity model

Automatic inverse diffusivity models have been proposed in previous works by Rommelaere et al. (1997) and Trudinger et al. (1997) and discussed in detail by Buizert et al. (2011). Specific requirements have to be considered to invert the direct model of gas transport in firns. First, as the optimization procedure iterates on (possibly non-physical) diffusivity profiles, the direct model has to be robust enough to undergo such trial profiles while providing relevant outputs. This motivated the proposed direct model established from mass conservation and first principles, along with the above numerical analysis. Secondly, the optimization method has to handle the system nonlinearities and a large data set (large-scale problem) with a limited number of measurements (under-determined system). Finally, the atmospheric scenarios and firn air measurements have to be consistent in terms of calibration scale and uncertainty estimates.

Supposing that the direct model is sufficiently robust and the data properly consistent, this section is focused on the inverse problem formulation and optimization performance evaluation.

3.1 Single gas problem formulation

The objective of the inverse diffusivity model is to determine the diffusivity profile that minimizes the difference between the simulated and measured mixing ratio $m_\alpha(z)$. This can be formulated as the distributed weighted nonlinear least squares problem:

$$D^*_\alpha(z) = \arg\min_{D_\alpha} \frac{1}{z_\mathrm{f}} \int_0^{z_\mathrm{f}} \frac{1}{\sigma_\alpha^2} \left(m_\alpha - \frac{\rho^\mathrm{o}_\alpha(z, t_\mathrm{f}, D_\alpha)}{\bar{\rho}^\mathrm{o}_\mathrm{air}(z)} \right)^2 \delta_\alpha dz$$

ACPD
11, 23029–23080, 2011

where $\sigma_\alpha(z)$ is the standard deviation of $m_\alpha(z)$ and $\delta_\alpha(z)$ is the Dirac delta function, set to one at the measurement location and 0 otherwise. The notation arg refers to the argument (the scalar space-dependent function $D_\alpha(z)$) that minimizes the considered cost function. The final time t_f corresponds to the measurement date (final value problem). The time dependency is omitted for air since only its steady-state behavior is considered, as mentioned previously. The gas densities ρ^o_α are obtained by solving Eq. (7) up to t_f and the air density $\bar{\rho}^o_{air}$ corresponds to the hydrostatic equilibrium. Additional constraints are necessary to ensure convergence, so we used $D > 0$ and $D_z < 0$ (i.e. diffusivity is monotically decreasing with depth, which results in a negative diffusivity gradient).

A specific analysis of this optimization problem and solution was proposed by Witrant and Martinerie (2010), where a dedicated variational approach was derived. Numerous optimization methods (e.g. optimization textbooks such as Kirk, 1970; Boyd and Vandenberghe, 2004; Mikles and Fikar, 2007 or more specifically Branch et al., 1999) are available to solve the discretized version:

$$D^*_\alpha = \arg\min_{D_\alpha} \frac{1}{N_m} \sum_{i=1}^{N_m} \frac{1}{\sigma^2_{\alpha,i}} \left(m_{\alpha,i} - \frac{\rho^o_\alpha(z_i, t_f, D_\alpha)}{\bar{\rho}^o_{air}(z_i)} \right)^2$$

where the i subscript denotes the measurements location and N_m is the number of measurements. The fact that a uniform grid is used to discretize the transport model implies an algorithm design where $m_{\alpha,i}$ is the sum of the actual measurement and the error induced by the mapping of the measurements to the discretization mesh (which depends on the interpolation method).

ACPD
11, 23029–23080, 2011

3.2 Multiple gases case

When multiple gases are considered simultaneously to constrain the effective firn diffusivity profile $D_{\text{eff}} = \{D_{\text{eddy}}, D_{\text{CO}_2}\}$, the inverse diffusivity problem becomes:

$$\text{RMSD}_j = \frac{1}{N_{\text{m},j}} \sum_{i=1}^{N_{\text{m},j}} \frac{1}{\sigma_{j,i}^2} \left(m_{j,i} - \frac{\rho_j^o(z_i, t_{\text{f}}, D_{\text{eff}})}{\bar{\rho}_{\text{air}}^{\text{o}}(z_i)} \right)^2 \tag{10}$$

$$D_{\text{eff}}^* = \min_{D_{\text{eff}}} \frac{1}{N_{\text{g}}} \sum_{j=1}^{N_{\text{g}}} \omega_j \text{RMSD}_j \tag{11}$$

where N_{g} is the number of gases considered, j denotes the specific trace gas considered and ω_j is a specific weight set on gas j. Solving the optimization problem, for example with a gradient descent algorithm, typically involves numerous runs of the direct model for each species with trial diffusivity profiles. This induces computational efficiency and robustness constraints on the direct model algorithm.

3.3 Algorithm overview

The inverse diffusivity model is obtained according to the algorithm presented in Fig. 2. First, for a given atmospheric scenario and D_{eff}, the direct model provides the trace gas density distribution at final time $\rho_j^{\text{o}}(z_i, t_{\text{f}}, D_{\text{eff}})$. The firn air measurements $m_{j,i}$ and related standard deviations (corrected to take into account the relative confidence in the scenarios) are then introduced to compute the weighted squared estimation error ϵ_j for each gas according to (10). The optimal diffusivity profile is finally obtained by iteratively updating D_{eff} to minimize the resulting global error according to (11).

The optimization method used to solve the minimization problem is a vector-valued approach, in the sense that a vector containing the squared errors at the different depth for each gas is provided to the algorithm. The under-determined aspect of the problem (fewer measurements than discretization depths for each gas) is artificially solved by

ACPD
11, 23029–23080, 2011

setting the errors to zero in the absence of measurement at the corresponding depths. The errors vector is used to compute a preconditioned conjugate gradient (numerical gradient computation from small variations on the diffusivity profile at each depth). The subspace trust-region method based on the interior-reflective Newton method (trust-region-reflective algorithm) described by Coleman and Li (1994, 1996) then determines the diffusivity profile evolution for the next iteration. The convergence rate is improved by starting from a coarse grid (e.g. $\Delta z = 0.8$ m) and increasing the resolution once a minimum is reached. This also allows for decreasing the impact of local minima. The non-uniqueness of the solution (unavoidable considering our limited data set) is illustrated in the results for each borehole presented in the Supplement by setting two different initial diffusivity profiles: one at zero and another set with a parameterized function. The variations in the final diffusivity are mainly limited to the upper firn and have no significant impact on the gas concentrations.

Specific care has to be taken with the standard deviation σ, as it has a direct impact on the optimal solution. This deviation has mainly two sources:

- the measurements deviation σ_{meas}, associated with the sampling conditions and measurement techniques;
- the impact of the scenario uncertainties σ_{scen} on the final distribution of the gas quantities, which necessitates running the direct model (7) (set with an approximation of D_α) with a given deviation of the atmospheric history.

Note that the deviation induced by the uncertainties on the measurements depths is neglected in this work. A finer description of the standard deviation computation is proposed by Buizert et al. (2011) and was used here for NEEM data. A similar methodology is used at other sites (the slight differences are described in the Supplement).

When setting the inverse diffusivity optimization based on multiple gases, the relative weights set on each gas ω_j can be considered as an extra degree of freedom. These weights can be set for example according to the inverse of the surface concentration, of the average or of the maximum value. It provides more weight on gases that have

ACPD
11, 23029–23080, 2011

a concentration increasing with depth, non cancelling at the bottom or with a high peak value, respectively, as illustrated in Fig. 3 for selected gases at NEEM (the full picture is given in the Supplement). The importance of these weights is related to the fact that the model cannot fit all data perfectly: different weightings consequently give more importance to different species. The most important differences occur in the LIZ (Fig. 3). Different models using the same specifications ($\omega_j = 1$) also lead to better/worse fit of different species (Buizert et al., 2011). With respect to other models, our (LGGE-GIPSA) model can be qualified as more *methane oriented*: it fits methane better than other species such as CH_3CCl_3 and $^{14}CO_2$ in their peak regions. Thus, setting ω_j to unity is used as a reference case but a gas-dependent definition could be of interest to obtain a diffusion profile that is more accurate to reconstruct atmospheric scenarios corresponding to a specific family of gases. For the objective of best constraining the firn diffusivity based on reference gases with different behaviors, setting $\omega_j = 0.5$ for two species with similar characteristics could also be considered. This is the case for CFC-11 and CFC-12 which have similar atmospheric histories and diffusion coefficients.

3.4 Reference and evaluation gases

The distinction between reference gases (used in the inverse diffusivity model optimization) and evaluation gases (which allow for discussing specific aspects of the physical model) is an important issue for the determination of the diffusivity profile. Indeed, the isotopic composition of gases with constant isotopic ratio (such as $\delta^{40}Ar$, $\delta^{86}Kr$ or $\delta^{15}N$) have a specific interest in our case as they are not affected by uncertainties on the atmospheric scenarios. They allow us to evaluate the almost-stagnant model behavior (lock-in region equilibrium and deviation from the gravitational slope). Nevertheless, their relatively low sensitivity to the diffusivity profile (gravitational fractionation is the main observed phenomenon in the diffusive region) and the specificity of their dynamics renders the choice of an appropriate weight with respect to the other gases particularly difficult. For this reason we chose not to use them in our diffusivity optimization.

ACPD
11, 23029–23080, 2011

Another motivation for not using inert gases for diffusivity optimization comes from the *system identification* theory (Ljung, 1999), which states that the system inputs (atmospheric scenarios and firn air measurements in our case) have to be "sufficiently rich" (in terms of frequency contents) to excitate all the model modes for a proper parameter identification. While the frequency content in atmospheric scenarios partially compensates the lack of measurements for gases with varying atmospheric conditions, the data set associated with gases that have a constant atmospheric concentration may not be informative enough and thus have a smoothing effect on the identified diffusivity, or at least not improve it. This was observed at NEEM where adding δ^{15}N as a reference gas did not significantly change the diffusivity profile or decrease the RMSD.

The relative weight of each gas used for the reference NEEM simulation are illustrated by the measurement signal to noise ratios (SNR, $m_{j,i}/\sigma_{j,i}$) in Fig. 4. Indeed, setting ω_j to unity in (10)–(11) weights the squared error of each measurement by $1/\sigma_{i,j}^2$ (with $\sigma_{i,j} = \sigma_{\text{meas},i,j} + \sigma_{\text{scen},i,j}$), normalized by the number of measurements per gas for the sum in (11). Gases with the highest SNR thus set the main model behavior. For the NEEM EU case with $\omega_j = 1$ for all gases, CH_4 is dominant up to 10 m while CO_2 has a major effect in the diffusive region. The reduced weight of CO_2 in the upper firn is due to the under-sampling of its seasonal variations (Buizert et al., 2011). In the lock-in region $^{14}CO_2$ contributes significantly (along with CO_2 and CH_4).

The final agreement between the firn model and specific data points is evaluated with the contribution of each measurement in the cost function. The results depicted on the right of Fig. 4 show the overall coherency of the model (only two points with a significantly higher cost) and the increased difficulty to obtain a coherent matching in the convective and lock-in regions.

3.5 Sensitivity to the use of multiple gases at NEEM

In order to characterize the efficiency and limitations of the multi-gas inverse diffusivity model, two tests are performed on NEEM EU data.

ACPD
11, 23029–23080, 2011

The first one, presented in Fig. 5, depicts the use of single gas optimized diffusivities on other gases (each reference gas is chosen in turn to compute the diffusivity). While a very good matching is obtained for the gas corresponding to the computed diffusivity, a large dispersion appears both on the diffusivity over the whole depth scale and on the other gases. It is interesting to note that the single gas diffusivity captures the best profile for each gas, which confirms that the inverse diffusivity problem is under constrained, for any single gas. The observed variability with single gas cases reflects the lack of information included in the associated data set, compensated by the multiple gas model (which captures the best fits except for the peaks on $^{14}CO_2$ and CH_3CCl_3). It is also interesting to note that the diffusivities for CFC-11 and CFC-113 are not significantly constraining the upper layers of the firn (flat diffusivity profiles), as their mixing ratios are particularly invariant there.

In the second test (Fig. 6) the inverse diffusivity model is run by removing one gas for each trial (the diffusivity thus results from 8 gases out of the 9 reference ones). The robustness of the inverse model (its ability to depict accurately the behavior of several gases) is strongly improved, with very limited variations of the diffusivity in the diffusive region of the firn. The remaining inconsistencies can possibly be induced by the 1-D hypothesis, the accuracy of gas diffusion coefficients, the measurements and scenarios uncertainties and the unmodeled transport phenomena. The upper region (top 15 m) still appears to be underconstrained as relatively large variations on the diffusivity do not induce significant deviations in the gas concentration distributions. It is interesting to note that CH_4 and $^{14}CO_2$ have an enhanced impact in the LIZ diffusivity. As these gases have a highly transient behavior in the lock-in region, they bring more information to the multigas model for this region than the other gases.

Similar conclusions can be drawn on the NEEM US borehole (see the single, double and triple gas results provided in the Supplement), where we can also observe that using two gases already brings a significant improvement in comparison to a single gas diffusivity.

ACPD
11, 23029–23080, 2011

3.6 Impulse response and the inverse scenario objective at NEEM

Age distributions can be considered as a model output of first interest for inverse scenario reconstruction, as discussed by Rommelaere et al. (1997) and Trudinger et al. (2002). The sensitivity of age distributions to the firn diffusivity thus provides an evaluation criterion for atmospheric trend reconstructions. Age distributions obtained from the impulse response of the model are presented for CO_2 at NEEM (EU hole) in Fig. 7. A convective zone test case is provided by comparing the case $\zeta = 4$ where the eddy diffusivity is set to zero with the reference case ($\zeta = 7$), as discussed in Sect. 2.9. While this clearly has a significant impact on the upper firn, the difference is relatively small below 60 m, especially near the age of maximum probability (maximum gain amplitude). Another test case is provided by setting the diffusivity to zero in the deep firn (when it becomes smaller than $0.05\,m^2\,yr^{-1}$, corresponding to the LIZ). The surface response is not affected but the responses below 70 m are significantly modified (13 % difference in the peak gain at 78.6 m). As most of the information for past history reconstruction older than 20 yr is contained below 65 m, diffusivity values in the upper firn are of secondary importance in comparison with the ones in the diffusive region and in the LIZ.

4 Trace gas transport at Arctic and Antarctic sites

In addition to NEEM-EU and NEEM-US, eleven firn air pumping operations previously modeled (Rommelaere et al. (1997), Fabre et al. (2000), Sowers et al. (2005), Faïn et al. (2009), Martinerie et al. (2009)) with the single-gas diffusivity minimization algorithm of Rommelaere et al. (1997) were simulated using our new multi-gas method. In this section, we try to decipher links between differences in their behaviors and major climatic characteristics of the drill sites: temperature and snow accumulation rate. Gaining knowledge about the relationship between firn physics and climate is important for the interpretation of trace gas records in ice cores (see e.g. Landais et al., 2006).

ACPD
11, 23029–23080, 2011

Firn models using a tuned diffusivity profile can be directly used only for present-day firn air pumping operations for which depth profiles of trace gases in firn are available. Modeling past firn profiles would require one to approximate their diffusivities with a simple parameterization dependent on climatic parameters.

4.1 δ^{15}N and gravitational behavior

An innovative aspect of our model developments is to explore the stagnant behavior of gases through the use of Darcy's law. In this section, our model results are compared with δ^{15}N data at the studied drill sites (Fig. 8) in order to evaluate the model capability of predicting the width of the LIZ. Thus we focus mainly on the deepest part of the δ^{15}N profiles. In the upper firn, δ^{15}N is affected by thermal diffusion driven by the seasonal variations of temperature (Severinghaus et al., 2001), a process not represented in our model. At intermediate depths, model results and δ^{15}N data (within uncertainties) primarily follow the gravitational slope. However the model deviates from the gravitational slope at the highest accumulation rate sites (DE08 and Devon Island). This confirms the observation of Trudinger et al. (1997) that faster firn sinking (advection) prevents δ^{15}N from reaching gravitational equilibrium.

Air occlusion in bubbles in the deep firn region was first observed by Schwander et al. (1993) on the mixing ratio and isotopic composition of nitrogen and oxygen. Battle et al. (1996) introduced the name of lock-in zone, defined as the deep firn region where δ^{15}N becomes constant instead of being enriched by gravitation. They associated the absence of gravitational enrichment to an absence of diffusive mixing. The LIZ is defined as the area between the lock-in depth (LID) and full bubble close-off depth (full COD, $f = 0$). Within experimental uncertainties, the model captures well the width of the LIZ. In our physical framework, it represents the area where gas transport becomes almost stagnant and implies equilibrium between Darcy's law and Fick's law. However, the effective firn diffusivity in the upper part of this region is still significant (see Sect. 4.2), as observed by Buizert et al. (2011) for the NEEM firn.

ACPD
11, 23029–23080, 2011

The width of the LIZ can be related to the diffusivity depth-gradient. Indeed, considering the transport Eq. (7) at steady-state ($[\rho^{\circ}_{\alpha} f]_t = 0$ and $\rho^{\circ}_{\alpha} = \rho^{\circ}_{\alpha,\mathrm{ss}}$) with the assumption that the gas is transported at the same speed as air ($w_\alpha = w_{\mathrm{air}}$, thus using the $A_{\mathrm{ss,sim}}$ simplification) implies:

$$[\rho^{\circ}_{\alpha,\mathrm{ss}} f (v + w_\alpha)]_z + \rho^{\circ}_{\alpha,\mathrm{ss}} (\tau + \lambda) - \left[D_\alpha \left([\rho^{\circ}_{\alpha,\mathrm{ss}}]_z + \frac{M_\alpha g}{RT} \rho^{\circ}_{\alpha,\mathrm{ss}} \right) \right]_z = 0$$

The first two terms cancel each other according to Darcy's equilibrium (as described in Sect. 2.6) and the previous equation simplifies to:

$$D_\alpha [\rho^{\circ}_{\alpha,\mathrm{ss}}]_{zz} + \left([D_\alpha]_z + D_\alpha \frac{M_\alpha g}{RT} \right) [\rho^{\circ}_{\alpha,\mathrm{ss}}]_z + \left([D_\alpha]_z \frac{M_\alpha g}{RT} + \lambda \right) \rho^{\circ}_{\alpha,\mathrm{ss}} = 0$$

Neglecting the first term (assuming small values of D_α and $[\rho^{\circ}_{\alpha,\mathrm{ss}}]_{zz}$ in the slow transport LIZ) and the radioactive decay, it appears that if the diffusivity gradient cancels in the LIZ, then the concentration gradient disappears (except in the null diffusivity case). Although this is a sufficient condition (rather than a necessary condition), it is confirmed by the observations made on Fig. 8, where the LIZ location is directly correlated to the region where the diffusivity gradient cancels. Note that additional tests based on the values or depth-gradients of the open porosity or the density did not lead to a clear correlation with the LID location. This phenomenon thus appears related to the firn tortuosity. It can be linked with the relationship $D_\alpha = f v D_{\alpha,\mathrm{g}}$ for a stagnant gas proposed by van Deemter et al. (1956) (see Sect. 2.5). The diffusivity depth-gradient then writes as:

$$[D_\alpha]_z = (f_z v + f v_z) D_{\alpha,\mathrm{g}}$$

Thus, as changes in f and f_z do not correlate with the LID, the LIZ specific transport should be related to the tortuosity. The fact that the concentration profile is not completely flat in the LIZ results from deviations from our previous hypotheses, which have thus to be considered as indications of the major physical trends.

ACPD
11, 23029–23080, 2011

Another important observation on Fig. 8 is that the width of the LIZ increases when snow accumulation increases (the main physical characteristics of the 13 modeled drill holes are summarized in Table 2). The most arid Antarctic plateau sites (Dome C and Vostok) virtually have no LIZ. The same behavior occurs at Megadunes (Severinghaus et al., 2010). Thus the δ^{15}N LIZ clearly does not represent the bubble close-off zone at these sites. As glacial periods are more arid than interglacial periods, the decreasing width of the δ^{15}N LIZ associated with the decrease of snow accumulation rate can generate a bias when trying to infer past bubble close-off depths from δ^{15}N data in ice cores (Landais et al., 2006; Dreyfus et al., 2010). In Table 2, we compare three definitions of the lock-in depth: the above δ^{15}N LID, the approximate depths at which a slope break is observed in the CO_2 and/or CH_4 depth profiles (called LID_{gas}, see e.g. Fig. 1) and the depth at which the closed/total porosity ratio is 10 % (called 10 % COD). δ^{15}N LID and LID_{gas} are consistent within uncertainties (2–3 m) except at Dome C and Vostok where they differ by 5–6 m. By contrast, the 10 % COD is deeper than δ^{15}N LID by 2 to 6 m at sites with 10 cm water equivalent per year or more snow accumulation, 10 % COD and δ^{15}N LID are approximately equal at sites with accumulation rates of about 7 cm water eq. yr^{-1}, and 10 % COD is about 10 meters higher than δ^{15}N at the lowest accumulation sites (< 4 cm). If the width of the LIZ defined by δ^{15}N or LID_{gas} appears related to the snow accumulation rate, the width defined by the 10 % COD shows a more erratic behavior (it varies between approximately 6 and 11 m without a clear link to the accumulation rate). However the model's open to closed porosity parameterization is scaled to the firn density profile and based on data at only three sites (Goujon et al., 2003), thus a better physical characterization of the LIZ associated with future firn air sampling programs would help improving the ice-core related understanding of firn physics.

ACPD
11, 23029–23080, 2011

4.2 Diffusivity profiles

Table 2 also provides quality indicators related to the diffusivity profile. The primary diagnostics is the root mean square deviation between model results and data for all gases used. However it is more difficult to fit simultaneously a large number of species than a small number of species, thus for example the RMSD is higher for NEEM-EU (nine gases) than NEEM-US (three gases). A useful complementary indicator is the difference between the minimum and maximum RMSD calculated with N-1 gases, this difference is 0.06 for NEEM-EU (the smallest of all sites) and 0.18 for NEEM-US.

Figure 9 compares the diffusivity profiles obtained for our 13 target drill holes. The fit of reference gases data at each site is illustrated in the Supplement, together with site-specific tests. In the upper firn (open porosity > 0.3) Vostok, North GRIP and NEEM-EU show higher diffusivities than other sites in relation with the occurrence of specific convective zone processes also indicated by δ^{15}N for Vostok (Bender et al., 1994) (13 m deep convective zone), NEEM-EU (Buizert et al., 2011) (~4 m deep convective zone), and North GRIP where nearly constant concentrations of several gases are observed in the top ~8 m (see Supplement). On the other hand Devon Island shows reduced diffusivities in most of the firn due to the presence of about 150 refrozen melt layers (see e.g. Martinerie et al., 2009). Although these heterogeneities are not modeled, the multi-gas diffusivity constraint brought a strong improvement at this site (see Supplement). Diffusivities at other sites than Devon Island are remarkably consistent for open porosities in the range 0.1–0.3. Understanding the deep firn results requires assessing where diffusivity becomes negligible. Sensitivity test were performed where firn diffusivity was set to zero when reaching different threshold values. Setting to zero the values of the firn diffusivity scaled by the CO_2 diffusion coefficient in free air (D_{eff}/D_{air}) which are lower than 10^{-3} has a significant impact on reference gas concentrations in all the LIZ, and on the δ^{15}N LID, whereas setting D_{eff}/D_{air} values lower than 10^{-4} to zero has a very small influence on the results. Thus the large range of model values below $D_{eff}/D_{air} = 10^{-4}$ are insignificant. For values of D_{eff}/D_{air} higher than about 10^{-3},

ACPD
11, 23029–23080, 2011

the decrease of diffusivity with decreasing open/closed porosity ratios is slowest for the lowest accumulation rate sites (Vostok and Dome C), shows intermediate values at South Pole and DML and is fast at other sites (the somewhat slower decrease at DE08 may be related to uncertainties due to the low sampling resolution in the LIZ for this early drill site). This is consistent with the accumulation rate dependent behavior of δ^{15}N illustrated in the previous section: higher diffusivities prevents gas transport from becoming stagnant.

Very young deep firn ages (see 50 % COD age in Table 2) calculated at Dome C and Vostok also support a fast gas transport at these sites. Note that very young gas ages were also calculated with the Rommelaere et al. (1997) model for Dome C (Martinerie et al., 2009). For other sites, the behavior of the 50 % COD age is more complex. It shows a general trend of increasing ages when accumulation decreases, which can be related to the advection speed: faster firn sinking induces a faster gas transfer from the open to the closed porosity of the ice. Some exceptions may be related to the variable thickness of the firns (e.g. younger ages at DML than South Pole). Other exceptions have no obvious explanation, such as the distinctly younger ages at Summit than other Arctic sites (North GRIP and NEEM), while these three sites have similar temperatures and accumulation rates and Summit is the deepest firn.

5 Conclusions

The process of trace gas transport in firns (direct model) was revised in the poromechanics framework, focusing on the transition to an almost-stagnant behavior in the lock-in region. A quasi-steady state approach allowed identifying advection-driven diffusivity processes as driving the trace gas concentrations equilibrium. The effect of molecular diffusion, and more precisely the turbulent behavior of gases (eddy flows) in the upper firn, was also investigated in relation with the convective layer behavior.

A new multi-gas constrained inverse model for diffusivity calculation, based on nonlinear least square minimization was described. The inverse problem formulation, impact of the optimization algorithm, choice of the reference gases and relative weights

ACPD
11, 23029–23080, 2011

were discussed. While the available measurements do not allow the inverse problem to be fully constrained, it was shown that the multi-gas approach greatly improves the efficiency of the inverse diffusivity model. Evaluation tools such as the signal to noise ratio of gas measurements, space distribution of the modeling errors and age distributions provided insights on the inverse model efficiency and limitations. More precisely, they allowed the relative effects of specific gases to be quantified and illustrated the fact that the diffusive region is more appropriately constrained than the convective and lock-in zones, in terms of the minimized modeling error (with respect to firn air measurements). Nevertheless, the observed variations in the convective zone have a negligible impact on the gases concentrations and the gas dynamics in the lock-in zone are appropriately represented by the model, even for trace gases with constant atmospheric concentrations. Despite two strong constraints in this approach: diffusivity decreases with depth and no eddy term is considered in the lock-in zone, this new model showed very good performance in a recent inter-comparison study (Buizert et al., 2011).

The proposed new model was applied to thirteen firn air pumping operations. The analysis of stable isotope ratios of molecular nitrogen (δ^{15}N) for the different sites allowed us to validate the capability of our model to predict the lock-in zone location. This region was shown to be associated with negligible depth-gradient diffusivity and qualitatively related to the accumulation rate. The reduced width of δ^{15}N (which defines the lock-in zone) at low accumulation rate sites also appears associated with higher diffusivities in the upper bubble close-off region. For the most arid sites, where no stagnant-gas area is observed, anomalously young mean gas ages are also obtained.

Future works investigating the deep-firn physics (e.g. tomography) and providing a temporal tracking of the upper firn behavior would be highly valuable to improve the understanding of these least well constrained parts of the firn. Evaluating the firn permeability depth-profile would also be of major interest to include the firn deformation gradient and temperature variations in the advection-driven diffusivity description, for both the steady-state and transient behaviors.

ACPD
11, 23029–23080, 2011

Supplementary material related to this article is available online at: http://www.atmos-chem-phys-discuss.net/11/23029/2011/acpd-11-23029-2011-supplement.pdf.

Acknowledgements. We are grateful to Jeffrey Severinghaus, Amaelle Landais and Christo Buizert for their useful comments on the paper and to Federico Bribiesca-Argomedo for his help in running numerical simulations. This work benefited greatly from numerous data available in public databases, in particular: AGAGE (http://cdiac.ornl.gov/ndps/alegage.html), NOAA ESRL (http://www.esrl.noaa.gov) and BADC (http://badc.nerc.ac.uk). We thank the people involved in the acquiring, analysis, and accessibility of these data. NEEM is directed and organized by the Center for Ice and Climate at the Niels Bohr Institute and US NSF, Office of Polar Programs. It is supported by funding agencies and institutions in Belgium (FNRSCFB and FWO), Canada (GSC), China (CAS), Denmark (FIST), France (IPEV, CNRS/INSU, CEA and ANR), Germany (AWI), Iceland (RannIs), Japan (NIPR), Korea (KOPRI), The Netherlands (NWO/ALW), Sweden (VR), Switzerland (SNF), United Kingdom (NERC) and the USA (US NSF, Office of Polar Programs). The French contribution to this study was further supported by CNRS through INSIS/PEPS-automatique and INSU/LEFE programs.

References

Anderson, J.: Fundamentals of Aerodynamics, McGraw-Hill Companies, 1991. 23049

Arnaud, L.: Modélisation de la transformation de la neige en glace à la surface des calottes polaires; étude du transport des gaz cans ces milieux poreux, Ph.D. thesis, Université Joseph Fourier, Grenoble, France, 1997. 23042

Battle, M., Bender, M., Sowers, T., Tans, P., Butler, J. H., Elkins, J. W., Ellis, J. T., Conway, T., Zhang, N., Lang, P., and Clarke, A.: Atmospheric gas concentrations over the past century measured in air from firn at the South Pole, Nature, 383, 231–235, 1996. 23059, 23079

Bender, M. L., Sowers, T., Barnola, J.-M., and Chappellaz, J.: Changes in the O_2/N_2 ratio of the atmosphere during recent decades reflected in the composition of air in the firn at Vostok Station, Antarctica, Geophys. Res. Lett., 21, 189–192, 1994. 23046, 23048, 23062, 23079

Boyd, S. and Vandenberghe, L.: Convex Optimization, Cambridge University Press, 2004. 23052

ACPD

11, 23029–23080, 2011

Branch, M., Coleman, T., and Li, Y.: A Subspace, Interior, and Conjugate Gradient Method for Large-Scale Bound-Constrained Minimization Problems, SIAM Journal on Scientific Computing, 21, 1–23, 1999. 23052

Bräunlich, M., Aballain, O., Marik, T., Jöckel, P., Brenninkmeijer, C., Chappellaz, J., Barnola, J.-M., Mulvaney, R., and Sturges, W.: Changes in the global atmospheric methane budget over the last decades inferred from ^{13}C and D isotopic analysis of Antarctic firn air, J. Geophys. Res., 106, 20465–20481, 2001. 23033

Buizert, C., Martinerie, P., Petrenko, V. V., Severinghaus, J. P., Trudinger, C. M., Witrant, E., Rosen, J. L., Orsi, A. J., Rubino, M., Etheridge, D. M., Steele, L. P., Hogan, C., Laube, J. C., Sturges, W. T., Levchenko, V. A., Smith, A. M., Levin, I., Conway, T. J., Dlugokencky, E. J., Lang, P. M., Kawamura, K., Jenk, T. M., White, J. W. C., Sowers, T., Schwander, J., and Blunier, T.: Gas transport in firn: multiple-tracer characterisation and model intercomparison for NEEM, Northern Greenland, Atmos. Chem. Phys. Discuss., 11, 15975–16021, doi:10.5194/acpd-11-15975-2011, 2011. 23032, 23033, 23046, 23048, 23051, 23054, 23055, 23056, 23059, 23062, 23064, 23070, 23072, 23079

Butler, J. H., Battle, M., Bender, M. L., Montzka, S. A., Clarke, A. D., Saltzman, E. S., Sucher, C. M., Severinghaus, J. P., and Elkins, J. W.: A record of atmospheric halocarbons during the twentieth century from polar firn air, Nature, 399, 749–755, 1999. 23033

Colbeck, S.: Air movement in snow due to windpumping, Journal of Glaciology, 35, 209–213, 1989. 23042

Coleman, T. and Li, Y.: On the Convergence of Reflective Newton Methods for Large-Scale Nonlinear Minimization Subject to Bounds, Mathematical Programming, 67, 189–224, 1994. 23054

Coleman, T. and Li, Y.: An Interior, Trust Region Approach for Nonlinear Minimization Subject to Bounds, SIAM Journal on Optimization, 6, 418–445, 1996. 23054

Coussy, O.: Poromechanics, John Wiley & Sons Ltd, 2nd edn., 2003. 23035, 23041, 23046

Cunningham, R. and Williams, R.: Diffusion in Gases and Porous Media, Plenum Press, New York, 1980. 23038

CRYOSTAT: CRYOspheric STudies of Atmospheric Trends in stratospherically and radiatively important gases (CRYOSTAT), available at: http://badc.nerc.ac.uk/data/cryostat (last access: January 2011), 2007. 23079

Dreyfus, G., Jouzela, J., Benderb, M., Landais, A., Masson-Delmottea, V., and Leuenberger, M.: Firn processes and $\delta^{15}N$: potential for a gas-phase climate proxy, Quaternary Sci. Rev.,

ACPD

11, 23029–23080, 2011

29, 28–42, 2010. 23061
Fabre, A., Barnola, J.-M., Arnaud, L., and Chappellaz, J.: Determination of gas diffusivity in polar firn: Comparison between experimental measurements and inverse modeling, Geophys. Res. Lett., 27, 557–560, 2000. 23033, 23039, 23058
Faïn, X., Ferrari, C. P., Dommergue, A., Albert, M. C., Battle, M., Severinghaus, J., Arnaud, L., Barnola, J.-M., Cairns, W., Barbante, C., and Boutron, C.: Polar firn air reveals large-scale impact of anthropogenic mercury emissions during the 1970s, P. Natl. Acad. Sci., 106, 16114–16119, doi:10.1073/pnas.0905117106, 2009. 23033, 23058
Firn Record of Trace Gases Relevant to Atmospheric Chemical Change over 100 yrs (FIRETRACC/100), available at: http://badc.nerc.ac.uk/data/firetracc (last access: January 2011), 2007. 23079
Freitag, J., Dobrindt, U., and Kipfstuhl, J.: A new method for predicting transport properties of polar firn with respect to gases on the pore-space scale, Ann. Glaciol., 35, 538–544, 2002. 23032, 23041
Goujon, C., Barnola, J.-M., and Ritz, C.: Modeling the densification of polar firn including heat diffusion: Application to close-off characteristics and gas isotopic fractionation for Antarctica and Greenland sites, J. Geophys. Res., 108, 4792, doi:10.1029/2002JD003319, 2003. 23037, 23061
Hörhold, M., Albert, M., and Freitag, J.: The impact of accumulation rate on anisotropy and air permeability of polar firn at a high-accumulation site, J. Glaciol., 55, 625–630, 2009. 23036, 23049
Kirk, D.: Optimal Control Theory: An Introduction, Electrical engineering, Prentice-Hall, Englewood Cliffs, New Jersey, 1970. 23052
Landais, A., Barnola, J.-M., Kawamura, K., Caillon, N., Delmotte, M., Van Omnen, T., Dreyfus, G., Jouzel, J., Masson-Delmotte, V., Minster, B., Freitag, J., Leuenberger, M., Schwander, J., Etheridge, D., and Morgan, V.: Firn-air δ^{15}N in modern polar sites and glacial-interglacial ice: a model-data mismatch during glacial periods in Antarctica?, Quaternary Sci. Rev., 25, 49–62, doi:10.1016/j.quascirev.2005.06.007, 2006. 23047, 23058, 23061, 23079
Laube, J. C., Martinerie, P., Witrant, E., Blunier, T., Schwander, J., Brenninkmeijer, C. A. M., Schuck, T. J., Bolder, M., Röckmann, T., van der Veen, C., Bönisch, H., Engel, A., Mills, G. P., Newland, M. J., Oram, D. E., Reeves, C. E., and Sturges, W. T.: Accelerating growth of HFC-227ea (1,1,1,2,3,3,3-heptafluoropropane) in the atmosphere, Atmos. Chem. Phys., 10, 5903–5910, doi:10.5194/acp-10-5903-2010, 2010. 23033

ACPD
11, 23029–23080, 2011

Ljung, L.: System Identification: Theory for the User, Information and System Sciences, PTR Prentice Hall, Upper Saddle River, NJ, 2nd edn., 1999. 23056
Martinerie, P., Lipenkov, V., Raynaud, D., Chappellaz, J., Barkov, N., and Lorius, C.: Air content paleo record in the Vostok ice core (Antarctica): a mixed record of climatic and glaciological parameters, J. Geophys. Res., 99, 10565–10576, 1994. 23042
Martinerie, P., Nourtier-Mazauric, E., Barnola, J.-M., Sturges, W. T., Worton, D. R., Atlas, E., Gohar, L. K., Shine, K. P., and Brasseur, G. P.: Long-lived halocarbon trends and budgets from atmospheric chemistry modelling constrained with measurements in polar firn, Atmos. Chem. Phys., 9, 3911–3934, doi:10.5194/acp-9-3911-2009, 2009. 23033, 23058, 23062, 23063
Mason, E. and Malinauskas, A.: Gas Transport in Porous Media: The Dusty-Gas Model, vol. 17, Chem. Eng. Monograph, Elsevier, New York, 1983. 23038
Mikles, J. and Fikar, M.: Process Modelling, Identification, and Control, Springer, 2007. 23052
Montzka, S. A., Kuijpers, L., Battle, M. O., Aydin, M., Verhulst, K. R., Saltzman, E. S., and Fahey, D. W.: Recent increases in global HFC-23 emissions, Geophys. Res. Lett., 37, L02808, doi:10.1029/2009GL041195, 2010. 23033
Montzka, S. A., Reimann, S. (Coordinating Lead Authors), Engel, A., Krüger, K., O'Doherty, S., Sturges, W., Blake, D., Dorf, M., Fraser, P., Froidevaux, L., Jucks, K., Kreher, K., Kurylo, M., Mellouki, A., Miller, J., Nielsen, O.-J., Orkin, V., Prinn, R., Rhew, R., Santee, M., Stohl, A., and Verdonik, D.: Scientific Assessment of Ozone Depletion: 2010, Global Ozone Research and Monitoring Project, Report No.52, 516 pp., chap. Ozone-Depleting Substances (ODSs) and Related Chemicals, Chapter 1, World Meteorological Organization, Geneva, Switzerland, 2011. 23033
Rommelaere, V., Arnaud, L., and Barnola, J.: Reconstructing recent atmospheric trace gas concentrations from polar firn and bubbly ice data by inverse methods, J. Geophys. Res., 102, 30069–30083, 1997. 23032, 23033, 23041, 23045, 23051, 23058, 23063
Schwander, J.: The Environmental Record in Glaciers and Ice Sheets, chap. The transformation of snow to ice and the occlusion of gases, 53–67, John Wiley, New York, 1989. 23032, 23041, 23044
Schwander, J., Barnola, J.-M., Andrié, C., Leuenberger, M., Ludin, A., Raynaud, D., and Stauffer, B.: The Age of the Air in the Firn and the Ice at Summit, Greenland, J. Geophys. Res., 98, 2831–2838, 1993. 23059
Schwander, J., Sowers, T., Barnola, J.-M., Blunier, T., Malaiz, B., and Fuchs, A.: Age scale of

ACPD
11, 23029–23080, 2011

the air in the summit ice: Implication for glacial-interglacial temperature change, J. Geophys. Res., 102, 19483–19494, 1997. 23036
Severinghaus, J. and Battle, M.: Fractionation of gases in polar ice during bubble close-off: New constraints from firn air Ne, Kr and Xe observations, Earth Planet. Sci. Lett., 474–500, 2006. 23041, 23048, 23079
Severinghaus, J., Grachev, A., and Battle, M.: Thermal fractionation of air in polar firn by seasonal temperature gradients, Geochem. Geophys. Geosyst., 2, 1048, doi:10.1029/2000GC000146, 2001. 23032, 23042, 23059
Severinghaus, J. P., Albert, M. R., Courville, Z. R., Fahnestock, M. A., Kawamura, K., Montzka, S. A., Mühle, J., Scambos, T. A., Shields, E., Shuman, C. A., Suwa, M., Tans, P., and Weiss, R. F.: Deep air convection in the firn at a zero-accumulation site, central Antarctica, Earth Planet. Sci. Lett., 293, 359–367, 2010. 23042, 23045, 23047, 23050, 23061
Sowers, T., Bernard, S., Aballain, O., Chappellaz, J., Barnola, J.-M., and Marik, T.: Records of the $\delta\ ^{13}C$ of atmospheric CH_4 over the last 2 centuries as recorded in Antarctic snow and ice, Global Biogeochem. Cy., 19, GB2002, doi:10.1029/2004GB002408, 2005. 23058
Stauffer, B., Schwander, J., and Oeschger, H.: Enclosure of air during metamorphosis of dry firn to ice, Ann. Glaciol., 6, 108–112, 1985. 23032
Thorstenson, D. and Pollock, D.: Gas Transport in Unsaturated Zones: Multicomponent Systems and the Adequacy of Fick's Laws, Water Resour. Res., 25, 477–507, 1989. 23040
Trudinger, C., Enting, L., Etheridge, D., Francey, R., Levchenko, V., Steele, L., Raynaud, D., and Arnaud, L.: Modeling air movement and bubble trapping in firn, J. Geophys. Res., 102, 6747–6763, 1997. 23032, 23045, 23051, 23059, 23079
Trudinger, C. M., Etheridge, D. M., Rayner, P. J., Enting, I. G., Sturrock, G. A., and Langensfelds, R. L.: Reconstructing atmospheric histories from measurements of air composition in firn, J. Geophys. Res., 107, 4780, doi:10.1029/2002JD002545, 2002. 23033, 23058
van Deemter, J., Zuiderweg, F., and Klinkenberg, A.: Longitudinal diffusion and resistance to mass transfer as causes of nonideality in chromatography, Chem. Eng. Sci., 5, 271–289, 1956. 23039, 23042, 23060
Webb, S. and Pruess, K.: The Use of Ficks Law for Modeling Trace Gas Diffusion in Porous Media, Transport in Porous Media, 51, 327341, 2003. 23038, 23050
Witrant, E. and Martinerie, P.: A Variational Approach for Optimal Diffusivity Identification in Firns, in: Proc. of the 18th Med. Conf. on Control and Automation, 892–897, Marrakech, Morocco, 2010. 23052

ACPD
11, 23029–23080, 2011

Table 1. Root mean square deviation between model results and firn data (RMSD, detailed in Sect. 3) associated with the choice of the transport model (NEEM EU and Vostok holes). The transport configuration ζ is defined in terms of non-Fick transport $\mathcal{A}_{ss}$, convection layer depth z_{conv}, lock-in depth z_{lid} and eddy diffusivity D_{eddy} threshold. [a] With a correction factor $\alpha_c = 0.6565$ to take into account the porosity effect (surface value); [b] $z_{eddy} = 10.6$ m. Note that the RMSD values presented here depend on the calibration of the data set and should be considered from a relative perspective. Recent updates in the calibration process explain the slight differences with the results presented in Buizert et al. (2011).

Site	ζ	$\mathcal{A}_{ss}$	z_{conv} (m)	z_{lid} (m)	D_{eddy} thres.	**RMSD**
NEEM	0	0	0	None	None	0.991
NEEM	1	$A_{ss,D}$	0	None	None	0.683
NEEM	2	$A_{ss,sim}$	0	None	None	0.689
NEEM	3	$\mathcal{A}_{ss,1}$	0	62.2	None	0.680
NEEM	4	$\mathcal{A}_{ss,2}$	4	None	None	0.698
NEEM	5	$\mathcal{A}_{ss,2}$	4	None	$\bar{D}_{CO_2,air}$	0.696
NEEM	6	$\mathcal{A}_{ss,2}$	z_{eddy} [b]	None	$\bar{D}_{CO_2,air}$	0.736
NEEM	7 (ref)	$\mathcal{A}_{ss,2}$	4	None	$\alpha_c \bar{D}_{CO_2,air}$ [a]	0.713
Vostok	2	$A_{ss,sim}$	0	None	None	0.432
Vostok	4	$\mathcal{A}_{ss,2}$	13	None	None	0.332
Vostok	7(ref)	$\mathcal{A}_{ss,2}$	13	None	$\alpha_c \bar{D}_{CO_2,air}$ [a]	0.322

ACPD
11, 23029–23080, 2011

Table 2. Physical characteristics of modeled firn air pumping sites. Devon Island, Summit, North Grip and NEEM are Arctic sites; other sites are Antarctic sites (DML stands for Dronning Maud Land). Major climatic parameters: snow accumulation rate (in centimeters water equivalent per year) and temperature are indicated in columns three and four. Columns 5 to 7 provide quality indicators for the diffusivity profiles: N_{gas} is the number of reference gases used for constraining diffusivity, the RMSD column provides the root mean square deviation between model results and data for the reference gases (the number between parentheses is the difference between the maximum and minimum RMSD calculated with $N_{gas} - 1$). Columns 8 to 12 provide indicators of the top and bottom heights of the LIZ: the last sampling (or measurement) depth, the model's full COD (open porosity is zero), LID_{gas} is the approximate depths at which a slope break is observed in the CO_2 and/or CH_4 depth profile (see e.g. Fig. 1), $\delta^{15}N$ LID is the depth at which $\delta^{15}N$ fractionation stops, 10 % COD and 50 % COD are the depths at which the closed/total porosity ratios are 10 % and 50 % respectively. The last column provides the mean age at 50 % COD.

Site	Drill year	Accu. (cm w eq)	Temp. (°C)	N_{gas}	RMSD	Last meas depth (m)	COD_{full} (m)	LID_{gas} (m)	$\delta^{15}N$ LID (m)	10 % COD (m)	50 % COD (m)	50 % COD age (yr)
DE08	1993	120	−19	5	0.57(0.10)	85	87	73	73	75.7	83.8	18
Devon Isl.	1998	30	−23	6	0.62(0.10)	59	59.8	48	51	52.6	57.7	48
Summit	2006	21	−32	6	0.70(0.15)	80	80.8	70	70	73.3	78.5	41
NEEM-EU	2008	20	−28.9	9	0.74(0.06)	77.8	78.8	63	63	68.3	75.8	64
NEEM-US	2008	20	−28.9	3	0.60(0.18)	75.6	78.8	63	63	68.3	75.8	65.5
North GRIP	2001	17	−31.5	7	0.79(0.09)	77.7	78.4	68	67	72.4	76.4	55.6
Berkner	2003	13	−26	7	0.87(0.10)	63	65.2	51	53	58.9	63.1	71
Siple	1997	10	−25.3	5	0.72(0.22)	56.5	57.6	48	49	51.1	55.6	50
South Pole	1995	7.4	−49.3	6	0.68(0.07)	122	123	112	114	112.3	119.4	72
South Pole	2001	7.4	−49.3	3	0.46(0.16)	121.6	123	112	112	113.1	119.4	75
DML	1998	7	−38	6	0.71(0.10)	72.8	76.8	68	70	68.9	74.3	60
Dome C	1999	3.6	−47	7	0.98(0.17)	99.5	100.4	95	100	91.2	97.6	32
Vostok	1996	2.2	−56	2	0.38(0.15)	100	101	95	101	90.5	97.9	25

ACPD
11, 23029–23080, 2011

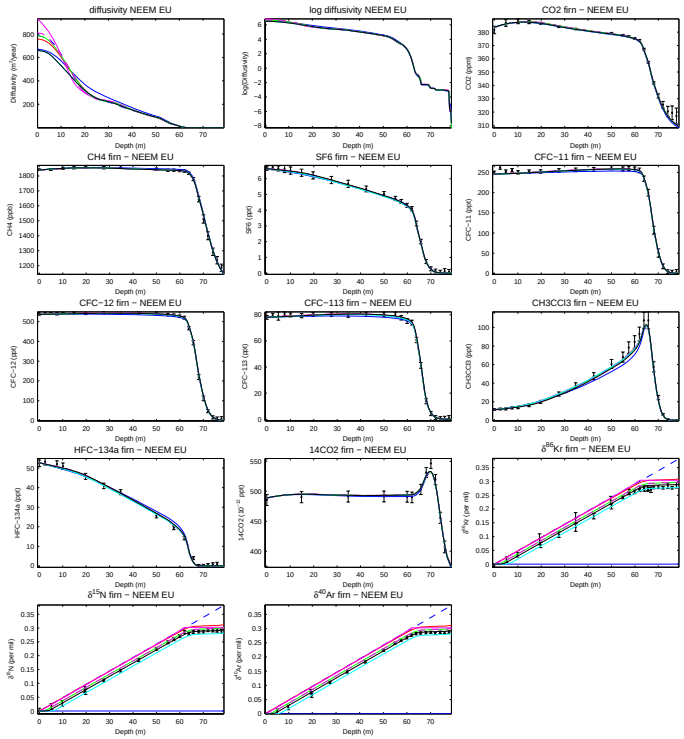

Fig. 1. Impact of the transport specification on the model results at NEEM (EU hole): Fick ($\zeta = 0$ blue "–"), QSS approximation and no convective region ($\zeta = 1$ in blue "- - -" and $\zeta = 2$ in red), QSS with convective (4 m) and lock-in regions ($\zeta = 3$, pink "–"), simplified QSS ($\zeta = 4$, green), simplified QSS with $z_{conv} = 4$ m and a maximum molecular diffusivity set by the one in free air ($\zeta = 5$, pink "- - -"), simplified QSS with $z_{conv} = z_{eddy}$ and a maximum molecular diffusivity set by the one in free air ($\zeta = 6$, turquoise), simplified QSS with $z_{conv} = 4$ m and a maximum molecular diffusivity corrected with the porosity ($\zeta = 7$, black, reference case). The NEEM firn air datasets (dots) are described in Buizert et al. (2011) together with the uncertainty (vertical bars) evaluation, which include both measurement and scenario uncertainties. δ^{15}N, δ^{40}Ar, δ^{86}Kr data were corrected for the effect of thermal diffusion.

ACPD
11, 23029–23080, 2011

Multi-gas transport in firn at eleven polar sites

E. Witrant et al.

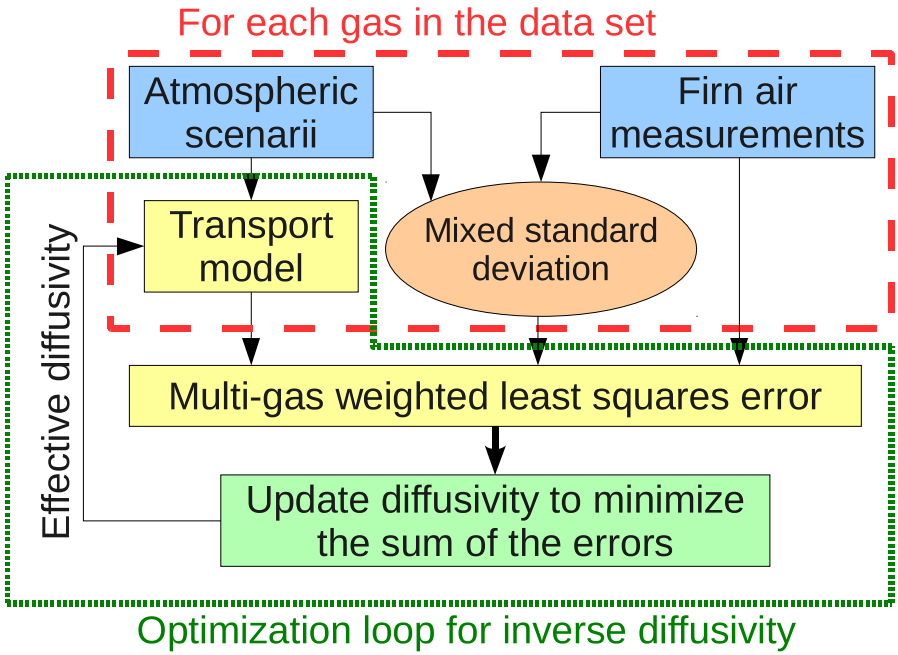

Fig. 2. Multi-gases inverse diffusivity algorithm.

ACPD
11, 23029–23080, 2011

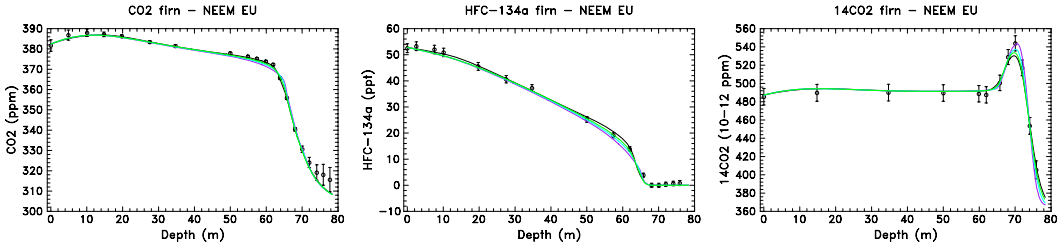

Fig. 3. NEEM concentration profiles (EU hole) for different cost function normalization approaches: with uncertainties (black, reference solution), surface concentration (purple), average concentration (turquoise) and maximum value (green).

ACPD
11, 23029–23080, 2011

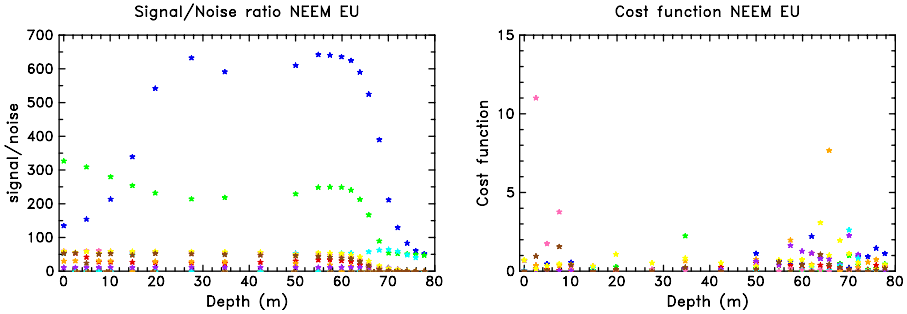

Fig. 4. Signal to noise ratio of firn air measurements (left) and data weights in the minimized cost function (right) at NEEM (EU hole) for CO_2 (blue), CH_4 (green), SF_6 (red), HFC-134a (orange), CH_3CCl_3 (violet), $^{14}CO_2$ (turquoise), CFC-11 (pink), CFC-12 (yellow) and CFC-113 (brown). The cost function distribution versus depth is presented for the reference case (one color per gas).

ACPD
11, 23029–23080, 2011

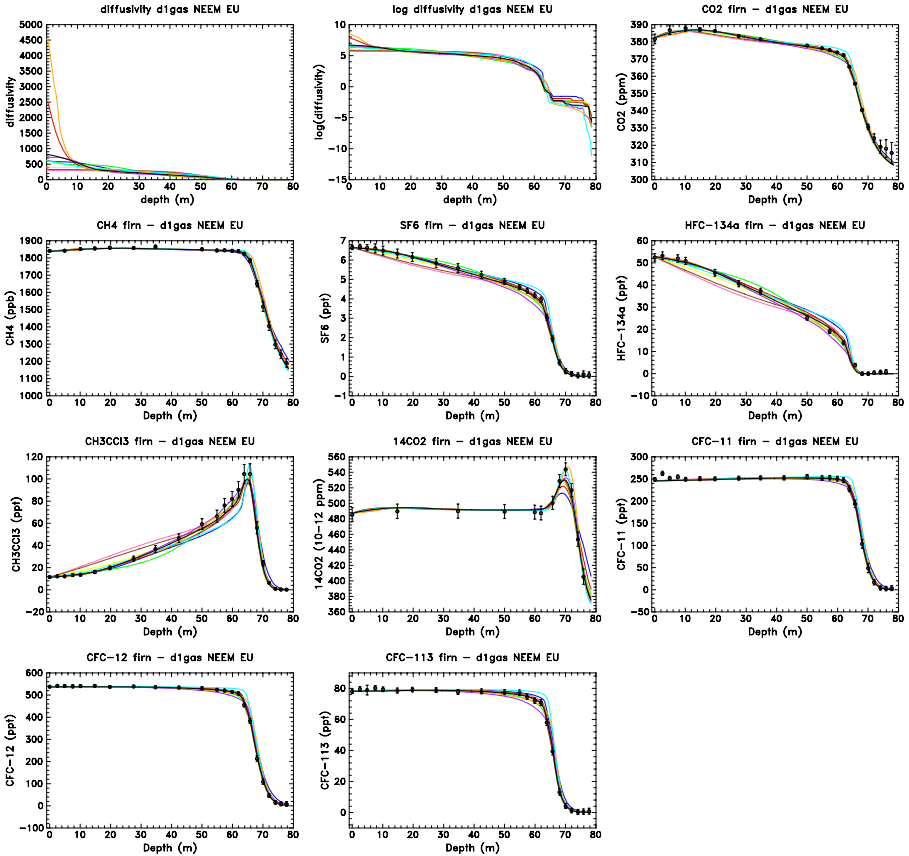

Fig. 5. Single gas inverse diffusivity model for NEEM (EU hole): each gas is used in turn to compute the diffusivity. Results for CO_2 (blue), CH_4 (green), SF_6 (red), HFC-134a (orange), CH_3CCl_3 (violet), $^{14}CO_2$ (turquoise), CFC-11 (pink), CFC-12 (yellow), CFC-113 (brown) and with the 9 gases (black, reference).

ACPD
11, 23029–23080, 2011

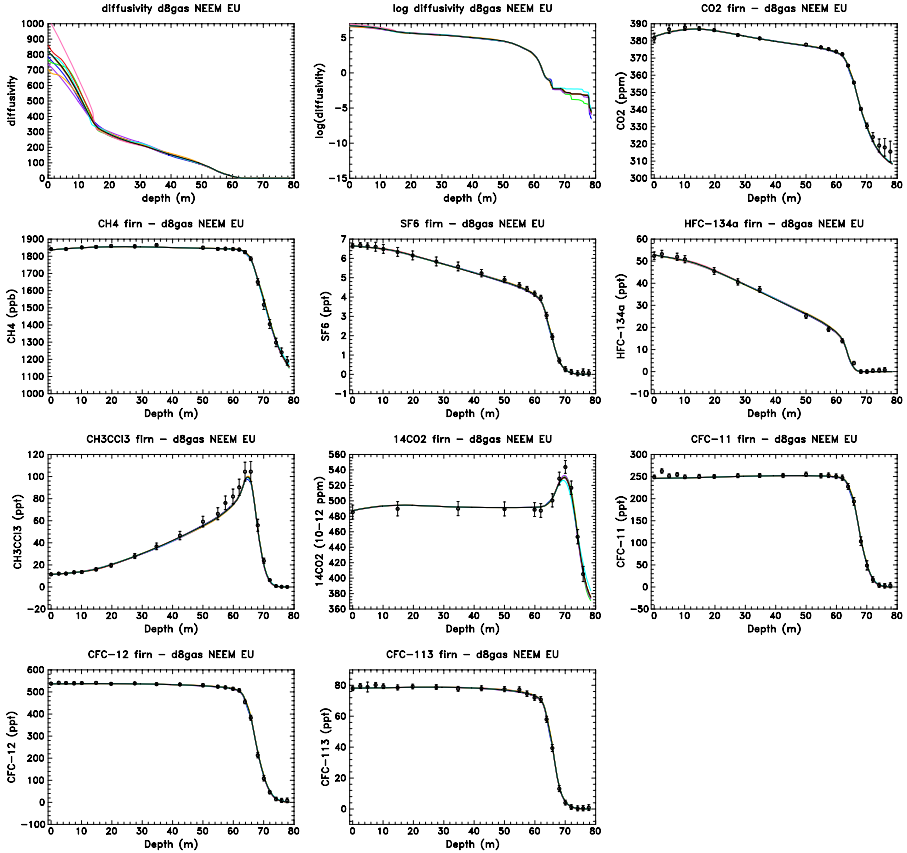

Fig. 6. Multiple gases inverse diffusivity model for NEEM (EU hole): the diffusivities are computed with 8 reference gases out of 9 (one gas removed for each test). The removed gases are CO_2 (blue), CH_4 (green), SF_6 (red), HFC-134a (orange), CH_3CCl_3 (violet), $^{14}CO_2$ (turquoise), CFC-11 (pink), CFC-12 (yellow), CFC-113 (brown) and none (black, reference).

ACPD
11, 23029–23080, 2011

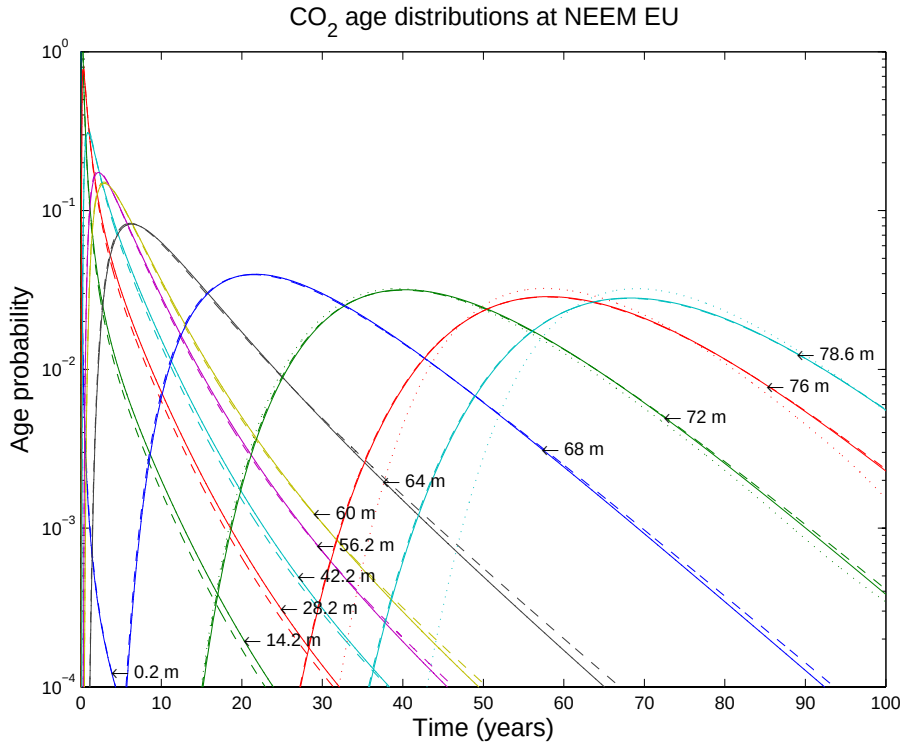

Fig. 7. Contribution of air of different ages at given depths (impulse response of the direct model for CO_2 at NEEM EU hole) using the optimal reference diffusivity ($\zeta = 7$, "–"), without eddy diffusivity ($\zeta = 4$, "- - -"), and with eddy diffusivity but canceling the diffusivity when $D < 0.05$ ("...").

ACPD
11, 23029–23080, 2011

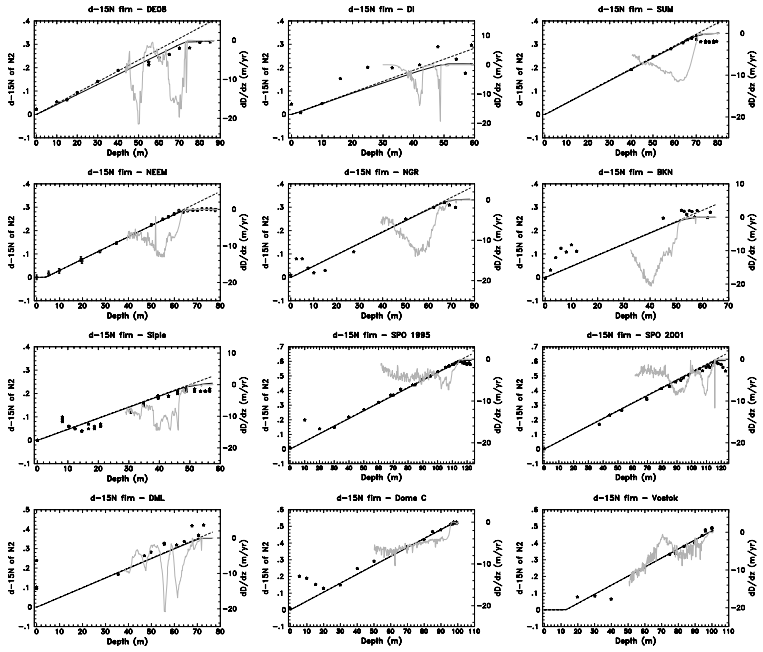

Fig. 8. Nitrogen (δ^{15}N of N_2) as a function of depth at different sites: measured ("*") versus modeled ("–") isotopic composition and comparison with the gravity slope ("- - -") and the diffusivity gradient (grey, right scale). d-15N stands for δ^{15}N of N_2 (in ‰). The firn air sampling sites are shown by order of decreasing snow accumulation rate (see Table 2). Experimental data for NEEM are corrected for the effect of thermal diffusion and are average results for the NEEM EU and NEEM US drill holes (Buizert et al., 2011). At other sites, deviations of δ^{15}N from the gravity slope in the upper firn are primarily explained by seasonal scale thermal diffusion. δ^{15}N data at Summit are from Severinghaus, private communication. Other datasets are from Bender et al. (1994), Battle et al. (1996), Trudinger et al. (1997), Landais et al. (2006), Severinghaus and Battle (2006), Buizert et al. (2011), FIRETRACC (2007) and CRYOSTAT (2007).

ACPD
11, 23029–23080, 2011

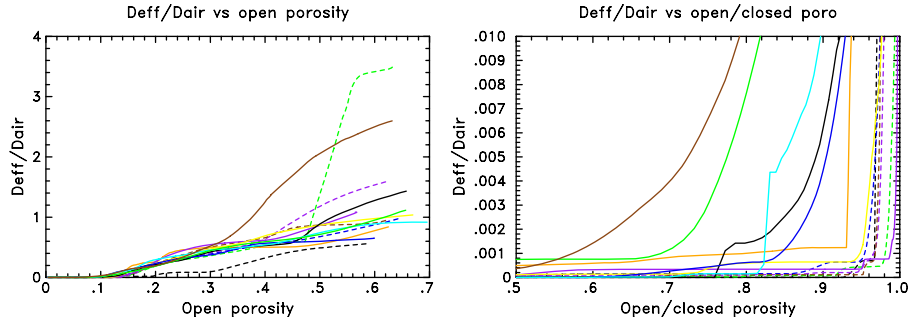

Fig. 9. Comparison of the diffusivity profiles calculated for the 13 drill holes considered. Deff/Dair is the ratio of firn diffusivity to the diffusion coefficient of CO_2 in free air. The left panel emphasizes the upper firn whereas the right panel emphasizes deep firn. Arctic sites are shown with dashed lines: Devon Island in black, Summit in blue, NEEM-EU in purple and NEEM-US in brown, North GRIP in green. Antarctic sites are shown as continuous lines: DE08 in orange, Berkner in purple, Siple in yellow, South Pole 1995 in dark blue, South Pole 2001 in light blue, Dronning Maud Land in black, Dome C in green and Vostok in brown.

ACPD
11, 23029–23080, 2011